NGA-East: Median Ground-Motion Models for the Central and Eastern North America Region

NGA-East: Median Ground-Motion Models for the Central and Eastern North America Region

ABSTRACT

This report documents recent ground motion models (GMMs) developed as part of the Next Generation Attenuation for Central and Eastern North America (CENA) project (NGA-East). NGA-East is a multi-disciplinary research project coordinated by the Pacific Earthquake Engineering Research Center (PEER) that involves a large number of participating junior and senior researchers, practitioners, and end-users. Various organizations have provided technical input to the project from academia, industry, and government agencies. The objective of NGA-East is to develop a new ground motion characterization (GMC) model for the Central and Eastern North America (CENA) region. The tectonic region of interest reaches across into Canada; thus, the term CENA instead of CEUS is used. The GMC consists in a set of new models (GMMs, a.k.a. GMPEs) for median, ground motions a set of standard deviation models, and their associated weights in the logic-trees, for use in probabilistic seismic hazard analyses (PSHA).

The current report documents the development of new median candidate GMMs. Models for standard deviations of ground motions are developed through a separate set of tasks within NGA-East and are published separately.

The GMMs have been developed using various tasks previously completed in NGA-East, notably the path regionalization, finite-fault simulations, and database development tasks. This report consists of eleven chapters. Each chapter has its own GMM developer team and may include multiple new GMMs. In all, a total of 20 GMMs are described in this report, covering a range of alternative approaches for modeling ground motions, building on empirical relations for CENA and WNA, using recorded ground motions and collected intensity data, and incorporating point-source and finite-fault simulations.

ACKNOWLEDGMENTS

LIST OF ACRONYMS

We have made an attempt to make the terminology as uniform as possible throughout the report. However, since each chapter is written by a different author or group of authors, we also tried to accommodate their personal style (e.g., passive versus active voice) and preferences. Some acronyms and symbols are also preferred by specific authors and reflected in their figure labels. We provide a list of the most common acronyms and symbols below and provide alternative notations when applicable.

ACR	Active Crustal Region
CBR	Center, body and range
CENA	Central and Eastern North America
GMC	Ground Motion Characterization
CEUS	Central and Eastern United States
CEUS SSC	Central and Eastern U.S. Seismic Source Characterization for Nuclear Facilities Project
DNFSB	Defense Nuclear Facilities Safety Board
DOE	United States Department of Energy
ENA	Eastern North America
EPRI	Electric Power Research Institute
FAS	Fourier Amplitude Spectra
FF, FFM	Finite Fault, Finite Fault Model
GM	Ground Motion
GMC	Ground Motion Characterization
GMM	Ground Motion Model is used preferably in the report, GMMs includes GMPEs and other model formats
GMPE	Ground Motion Prediction Equation is used for GMMs that have been parameterized into equations
GMIM	Ground Motion Intensity Measure (PSA, PGA, PGV)
M	Moment magnitude
NGA	Next Generation Attenuation
NGA-East	Next Generation Attenuation Relationship for the Central and Eastern North American Region
NGA-West	Next Generation Attenuation Relationship for shallow crustal earthquakes in active tectonic regions (original project)
NGA-West2	Next Generation Attenuation Relationship for shallow crustal earthquakes in active tectonic regions (phase 2 of NGA-West project)
NRC	United States Nuclear Regulatory Commission
NUREG	Regulatory guides, reports and brochures from the U.S. Nuclear Regulatory Commission
PGA	Peak Ground Acceleration
PGV	Peak Ground Velocity
PIE	Potentially-Induced Event
PS, PSM	Point-Source, Point-Source Model
PSA, SA	Pseudo-Spectral Acceleration (5% damping in this report), some modelers use SA (Spectral Acceleration) instead

PSHA	Probabilistic Seismic Hazard Analysis
Q	Quality factor
R_{HYP}, R_{hyp}	Hypocentral distance (km)
R_{JB}, R_{jb}	Joyner-Boore distance: closest distance to horizontal projection of fault trace (km)
R_X	Equivalent to Joyner-Boore distance measured perpendicularly to the fault trace (km). R_X is negative on the footwall side of the fault and positive on the hanging-wall side
R_{RUP}, R_{rup}, R_{clst}	Rupture distance: closest distance to the fault trace (km)
$RotD_{50}$	Median value of resultants of two horizontal components of ground motions as computed over each angle of rotation from 1 to 180°
SCR	Stable Continental Region
SSC	Seismic Source Characterization
SSHAC	Senior Seismic Hazard Assessment Committee
T	Spectral period (in seconds)
TDI	Technically Defensible Interpretations
TI	Technical Integrator
U.S.	United States
USGS	United States Geological Survey
V_S	Shear-wave velocity
V_{S30}	Time-averaged shear-wave velocity in top 30 meters of geomaterial
WG	Working Group
WUS	Western United States
Z_{HYP}, Z_{hyp}	Depth to hypocenter (km)
Z_{TOR}	Depth to top of rupture (km)

CONTENTS

1   Introduction

Christine A. Goulet, Yousef Bozorgnia

Pacific Earthquake Engineering Research Center (PEER)
University of California, Berkeley

Norman A. Abrahamson

Pacific Gas and Electric Company
San Francisco, California

1.1   BACKGROUND

This report documents recent ground motion models (GMMs) developed as part of the Next Generation Attenuation for Central and Eastern North America (CENA) project (NGA-East). NGA-East is a multi-disciplinary research project coordinated by the Pacific Earthquake Engineering Research Center (PEER) that involves a large number of participating researchers, practitioners, and end-users from various organizations in academia, industry, and government.

The objective of NGA-East is to develop a new ground motion characterization (GMC) for the CENA region. The GMC consists of a set of new GMMs (a.k.a. GMPEs) for median ground motions, a set of standard deviation models, and their associated weights in the logic-trees, for use in probabilistic seismic hazard analyses (PSHA). The current report documents the development of new median GMMs. Models for standard deviations of ground motions are developed through a separate set of tasks within NGA-East and are published separately. The term GMM is used as the general term in this report. Some models have been parameterized into equations, and the term "ground-motion prediction equations (GMPE)" is applicable, and other models consist of sets of ground-motions tables. The term GMM is general and applicable to all the models.

1.2   NGA-EAST MODEL DEVELOPMENT CONSTRAINTS

The NGA-East objective is to develop a comprehensive GMC for CENA. The project constraints have been developed to address the key earthquake scenarios identified in the CEUS Seismic Source Characterization project [EPRI/DOE/NRC 2012].

The magnitude used in NGA-East is the Moment Magnitude, **M**. **M** is related to seismic moment, M_0, by Hanks and Kanamori [1979] as:

$$\mathbf{M} = 2/3\log(M_0 \text{ in dyne-cm}) - 10.7 \tag{1.1}$$

Median GMMs are to provide "average" horizontal ground motions on very hard-rock (VHR) sites located up to 1200 km from future earthquakes in CENA, with **M** in the 4.0 to 8.2 range. The VHR reference site conditions have been defined by the NGA-East Geotechnical Working Group as corresponding to shear-wave velocity V_S = 3000 m/sec and a kappa (κ) of 0.006 sec. The development of the reference sites conditions is detailed in two PEER reports: Hashash et al. [2014a] and Campbell et al. [2014]. In addition, the GMM developers have focused the development of their models on the CENA region that excludes the Gulf Coast (see Region 1, or GROUP 2; see Section 1.3.1.2). The GMMs for the Gulf Coast are developed in separate NGA-East tasks. Also, the GMMs documented in this report are for footwall condition, and adjustments for hanging-wall condition are developed in a separate task.

The preferred "average" horizontal ground-motion intensity measure (GMIM) is RotD$_{50}$ [Boore 2010]. RotD$_{50}$is the median value of resultants of two horizontal components of ground motions as computed over each angle of rotation from 1 to 180°. RotD$_{50}$ is computed independently for each spectral period/frequency. The minimum requested GMIMs are peak ground acceleration (PGA), peak ground velocity (PGV), and 5%-damped linear pseudo-spectral acceleration (PSA) for oscillator periods listed in Table 1.1.

Table 1.1   Minimum 5%-damped PSA periods (and frequencies) for NGA-East GMM development

T (sec)	F(Hz)
0.01	100
0.02	50
0.025	40
0.03	33.33
0.04	25
0.05	20
0.075	13.33
0.1	10
0.15	6.67
0.2	5
0.25	4
0.3	3.33
0.4	2.5
0.5	2
0.75	1.33
1	1
1.5	0.67
2	0.5
3	0.33
4	0.25
5	0.2
7.5	0.13
10	0.1

1.3 DATASETS AND MODEL BUILDING TOOLS

The NGA-East GMM developers had access to a series of datasets and modeling tools. Specific references to those are provided within the different chapters. Summary of the key products are elaborated in the following sub-sections.

1.3.1 NGA-East Database

1.3.1.1 Summary and Attributes

The NGA-East ground-motion database includes the two- and three-component ground-motion recordings from numerous selected events ($\mathbf{M} > 2.5$, distances of 2000 km or more) recorded in the CENA region since 1988 [Goulet et al. 2014]. This is the largest database of processed ground motions recorded in stable continental regions (SCRs). It contains over 29,000 records from 81 earthquake events at 1379 recording stations. The database includes PSA for the 5%-damped elastic oscillators, with periods ranging from 0.01 to 10 sec. As indicated Section 1.2, the preferred GMIM used for the NGA-East GMM development is RotD_{50}, which is also provided for the same period range. The NGA-East database consists of three groups of complementary products: the summary file referred to as the "flatfile," which contains metadata, ground-motion information and GMIM, the time series (acceleration, velocity, and displacement), and the corresponding Fourier spectra files. The flatfile as well as additional requested products were shared with all the GMM developers.

1.3.1.2 Regionalization

A separate task in NGA-East was to regionalize CENA on the basis of systematic differences in simulated ground motions and their attenuation. From this task four distinct regions were defined as follows [Dreiling et al. 2014]:

1. Mississippi Embayment/Gulf Coast region (MEM)
2. Central North America (CNA)
3. The Appalachian Province (APP)
4. The Atlantic Coastal Plain (ACP)

These four regions are shown in Figure 1.2, with the numbering used in the NGA-East flatfile (Section 1.3.1.1). The flatfile includes three separate fields for regionalization. The first two, correspond to the "Event and Station Region Number," respectively. For these two fields, the number directly corresponds to the region containing the epicenter (Event Field) and the station (Station Field). If the epicenter or the station is outside these four regions, the flag is set to -999.

The third and last regionalization field is called "Path Region Number" and aims to define a region containing the full propagation path (from the epicenter to the Station). If the full path is contained within any of the four regions above, the field is populated with the region number directly. If either or both of the Event or Station Region Number are outside the four regions (at least one of the fields is -999), then the Event Station Field is also -999.

The regionalization task also demonstrated that the four regions could be aggregated into two distinct attenuation groups:

GROUP 1: Central North America (CNA), Appalachians (APP), and Atlantic Coastal Plain (ACP)

GROUP 2: Mississippi Embayment/Gulf Coast (MEM or GC)

Two new regions were created to accommodate this grouping of regions. Region 5 includes paths that cross any or many of the regions' 2, 3, and 4 boundaries. To fully populate the attenuation Group 1 from above, one would have to combine data with Path Region numbers 2, 3, 4, and 5. Region 6 allows for paths crossing between any sub-region of Group 1 into region 1 (MEM/GC).
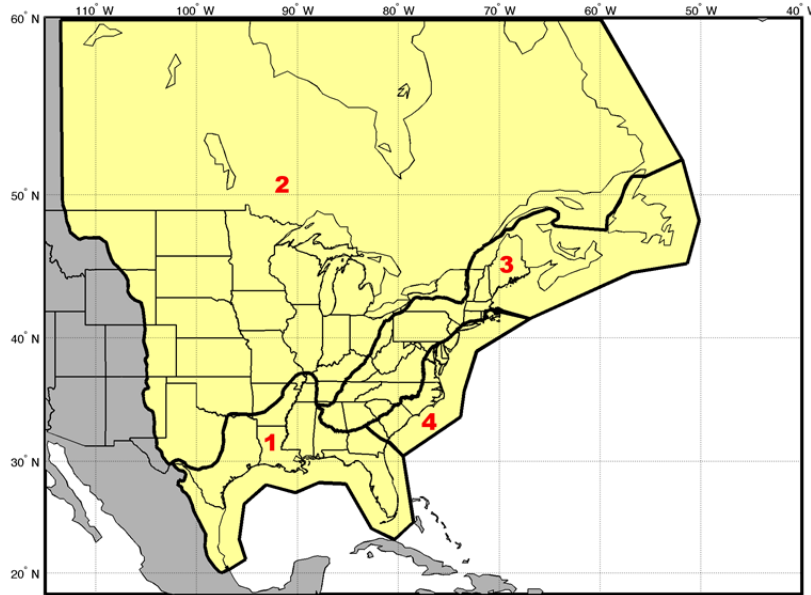
Figure 1.2 Four regions defined for Central and Eastern North America (CENA). The regions have been numbered as follows for the NGA-East database: (1) Mississippi Embayment/Gulf Coast region; (2) central North America; (3) the Appalachian Province; and (4) the Atlantic Coastal Plain.

1.3.2 NGA-East Site Conditions Corrections

The NGA-East database includes V_{S30} estimates for all the recording stations. However, only about 100 sites have V_{S30} values from *in situ* measurements. The vast majority of stations were assigned an inferred V_{S30} value based on various proxy methods described in Chapter 5 of Goulet et al. [2014]. Therefore, there is a certain level of uncertainty on the estimated V_{S30} values, rendering the correction to reference rock also uncertain.

The approach favored by NGA-East was to let each GMM modeling group use their own site correction methods for correcting the as-recorded ground motions to the reference site condition. With this approach, a wider range of ground motions is essentially captured. The GMM developers were nonetheless provided with a draft version of the Boore [2015] report on

site correction models for Fourier amplitude spectra (FAS) and PSA. This was used as a verification tool or as part of the model building process by the different GMM modeling teams.

1.3.3 CENA Models for Attenuation

NGA-East compiled a series of attenuation models from the literature. By attenuation models, we refer to correlated models of geometrical spreading and anelastic attenuation (Q) from ground-motions studies and not to complete GMMs. Expecting to have GMMs based on the point-source stochastic model developed as part of the project, the NGA-East team wanted to select a subset of attenuation models that would (1) span the range of models available and (2) be small enough to be manageable.

The initial literature review contained over 40 models developed between 1983 and 2014 (see Appendix 1A). From this list, a subset of 22 models was selected based on the quality and age of the data used in the published studies. Another review of these 22 models was completed, and six models were selected as representative of the range of available models (see Appendix 1A). The six selected models are listed in Table 1.2.

Table 1.2   Summary of the selected representative attenuation models.

Model and Reference	Geometric Spreading $G(R)$	What is "R"?[1]	Attenuation $\exp(-\pi f R/Q\beta)$	Applicable Range[2]
AB95 (J97) [Atkinson and Boore 1995]	$G(R) = \begin{cases} R^{-1}, & R \leq 70 \text{ km} \\ C_0 R^0, & 70 \text{ km} < R \leq 130 \text{ km} \\ C_1 R^{-0.5}, & R > 130 \text{ km} \end{cases}$ $C_0 = (1/70)$, $C_1 = (130^{0.5}/70)$	$R = R_{hyp}$	$Q(f) = 680f^{0.36}$ $\beta = 3.8$ km/sec	$4.0 \leq \mathbf{M} \leq 7.25$ $10 \leq R \leq 500$ km $0.5 \leq f \leq 20$ Hz
SGD02 (S02sc, EPRI93) [Silva et al. 2002]	$G(R) = \begin{cases} R^{-(a+b(\mathbf{M}-6.5))}, & R \leq 80 \text{ km} \\ C_0 R^{-0.5(a+b(\mathbf{M}-6.5))}, & R > 80 \text{ km} \end{cases}$ $a = 1.0296$, $b = -0.0422$, $C_0 = 80^{-0.5(a+b(\mathbf{M}-6.5))}$	$R = R_{hyp}$	$Q(f) = 351f^{0.84}$ $\beta = 3.52$ km/sec	$4.5 \leq \mathbf{M} \leq 8.5$ $1 \leq R \leq 400$ km $0.1 \leq f \leq 100$ Hz
A04 (BCA10a) [Atkinson 2004]	$G(R) = \begin{cases} R^{-1.3}, & R \leq 70 \text{ km} \\ C_0 R^{0.2}, & 70 \text{ km} < R \leq 140 \text{ km} \\ C_1 R^{-0.5}, & R > 140 \text{ km} \end{cases}$ $C_0 = (70^{-0.2}/70^{1.3})$, $C_1 = C_0(140^{0.5}/140^{-0.2})$	$R = R_{hyp}$	$Q(f) = \max(1000, 893f^{0.32})$ $\beta = 3.7$ km/sec	$4.4 \leq \mathbf{M} \leq 6.8$ $10 \leq R \leq 800$ km $0.05 \leq f \leq 20$ Hz
BCA10d [Boore et al. 2010]	$G(R) = R^{-1}$ all R	$R = R_{PS}$	$Q(f) = 2850$ $\beta = 3.7$ km/sec	$4.4 \leq \mathbf{M} \leq 6.8$ $10 \leq R \leq 800$ km $0.05 \leq f \leq 20$ Hz
BS11 [Boatwright and Seekins 2011]	$G(R) = \begin{cases} R^{-1}, & R \leq 50 \text{ km} \\ C_0 R^{-0.5}, & R > 50 \text{ km} \end{cases}$ $C_0 = (50^{0.5}/50)$	$R = R_{hyp}$	$Q(f) = 410f^{0.5}$ $\beta = 3.5$ km/sec	$4.4 \leq \mathbf{M} \leq 5.0$ $23 \leq R \leq 602$ km $0.2 \leq f \leq 20$ Hz
AB14 [Atkinson and Boore 2014]	$G(R) = \begin{cases} 10^{T_c C_{LF}} R^{-1.3}, & R \leq 50 \text{ km} \\ C_0 R^{-0.5}, & R > 50 \text{ km} \end{cases}$ $T_c = \begin{cases} 1, & f \leq 1 \text{ Hz} \\ 1 - 1.429 \log_{10}(f), & 1 \text{ Hz} < f < 5 \text{ Hz} \\ 0, & f \geq 5 \text{ Hz} \end{cases}$ $C_{LF} = \begin{cases} 0.2 \cos\left[\frac{\pi}{2}\left(\frac{R-h}{1-h}\right)\right], & R \leq h \\ 0.2 \cos\left[\frac{\pi}{2}\left(\frac{R-h}{50-h}\right)\right], & h < R < 50 \text{ km} \end{cases}$ h = focal depth (km), $C_0 = (50^{0.5}/50^{1.3})$	$R = R_{PS}$	$Q(f) = 525f^{0.45}$ $\beta = 3.7$ km/sec	$3.5 \leq \mathbf{M} \leq 6$ $10 \leq R \leq 500$ km $0.2 \leq f \leq 20$ Hz

[1]R_{hyp} = hypocentral distance; R_{PS} = effective point source distance
   $R_{PS} = [R_{hyp}^2 + h_{FF}^2]^{1/2}$, $\log_{10}(h_{FF}) = -0.405 + 0.235\mathbf{M}$ [Yenier and Atkinson 2015a]

[2]When applicable range not explicitly stated in paper it was inferred from data comparisons.

1.3.4 CENA Finite-Fault Simulations and Data

Following a large finite-fault validation exercise, three finite-fault simulations modeling approaches passed the acceptance criteria and were selected for the generation of CENA ground-motion data. The methodologies are implemented on the Southern California Earthquake Center Broadband Platform (SCEC BBP), version 14.6, and are documented, along with the validation exercise itself, in a Focus Section in *Seismological Research Letters* (Volume 86, Issue 1). The simulations methodologies were evaluated for applicability to Western U.S. (WUS), Japanese, and CENA events, as detailed in Goulet et al. [2015], Maechling et al. [2015] and Dreger et al. [2015].

The EXSIM (EX), Graves and Pitarka (GP) and San Diego State University (SD) methodologies were selected for NGA-East and are described in detail in Atkinson and Assatourians [2015], Graves and Pitarka [2015], and Olsen and Takedatsu [2015]. The NGA-East project was in agreement with Dreger et al. [2015] that the ground motions from these methods should not be used for their absolute values, but instead for their relative magnitude scaling effects on ground motions. NGA-East developed a set of simulation scenarios for that purpose. The different earthquake scenarios and station layouts were defined to capture the effect of **M**-scaling relative to **M**=5, for a range of distances.

Appendix 1B summarizes the simulations process and links to data files for the **M**-scaling models.

1.3.5 NGA-West2 Database

A subset of GMM developers used data from active crustal regions (ACRs) and developed parts of their model using the NGA-West2 database [Ancheta et al. 2014]. The NGA-West2 database includes earthquake events from multiple ACRs, such as from the WUS, Middle East, Japan, and China, among others. The key NGA-West2 product used in the NGA-East GMM development was the flatfile, which includes metadata on source, propagation and site effects as well as 5%-damped PSA $RotD_{50}$ values.

1.4 MODELING APPROACHES AND REPORT ORGANIZATION

1.4.1 Organization by Type of Modeling Approach

This report consists of a collection of individual chapters, each authored by the GMM developer teams (or groups of developers). Each chapter, therefore, provides a self-contained documentation of the models and suites of models. The NGA-East project organized the methods by a general type, based on the approach used in the development, as briefly summarized below.

Table 1.3 summarizes the outline of the report, with each GMM or suite of GMMs organized based on the modeling approach, the set of seismological constraints, and the extrapolation approach for large **M**, close-in distance and higher frequencies.

Approach: This column summarizes the general underlying modeling approach. For example, we distinguish models that are essentially empirical, based on point-source (PS) or finite-fault (FF) simulations, from those that use the hybrid empirical method (HEM).

Constraints: This provides further information on how the model development is constrained, which can be based on seismological models or on ground-motion data.

Extrapolation: This refers to how the models extrapolate beyond the NGA-East database.

Table 1.3   Summary of GMM approaches covered in this report.

Approach	Constraints	Extrapolation	Chapter Number, Title (Authorship)
Traditional Point-Source (PS) Stochastic (FAS-based)	PS model, published sets of empirical attenuation models, NGA-East database	PS model	2. Point-Source Stochastic-Method Simulations of Ground Motions for the PEER NGA-East Project (D.M. Boore)
	PS model, broadband inversion of NGA-East database	PS model	3. Development of Hard Rock Ground-Motion Models for Region 2 of Central and Eastern North America (R.B. Darragh, N.A. Abrahamson, W.J. Silva, and N. Gregor)
Regionally-Adjustable Generic GMM based on Point-Source model (PS Referenced Empirical)	PS model used to develop generic GMM, parameters defined from data-rich host region, adjustments using NGA-East database	Generic GMM adjusted to CENA data	4. Regionally-Adjustable Generic Ground-Motion Prediction Equation based on Equivalent Point-Source Simulations: Application to Central and Eastern North America (E. Yenier and G.M. Atkinson)
Hybrid Empirical (FAS- and PSA-based)	Published sets of CENA and WUS PS models	GMM host region (WUS)	5. Ground-Motion Prediction Equations for Eastern North America using a Hybrid Empirical Method (S. Pezeshk, A. Zandieh, K.W. Campbell, and B. Tavakoli)
Finite-Fault (FF)Simulations (PSA-based)	FF model, NGA-East database	FF model	6. Ground-Motion Predictions for Eastern North American Earthquakes Using Hybrid Broadband Seismograms from Finite-Fault Simulations with Constant Stress-Drop Scaling (A. Frankel)
			7. Hybrid Empirical Ground-Motion Model for Central and Eastern North America using Hybrid Broadband Simulations and NGA-West2 GMPEs (A. Shahjouei and S. Pezeshk)
Traditional Empirical (PSA-based)	NGA-East database	Intensity	8. Empirical Ground -otion Prediction Equations for Eastern North America (M.N. Al Noman and C.H. Cramer)
		Imposed spectral shape	9. Ground-Motion Prediction Equations for the Central and Eastern United States (V. Graizer)
Referenced Empirical (PSA-based)	NGA-East database	GMM host region (WUS)	10. Referenced Empirical Ground-Motion Model for Eastern North America (B. Hassani and G.M. Atkinson)
FAS-RVT-PSA Empirical (require FAS and duration models)	NGA-East database	PS and FF models for scaling, Global GMs for extrapolation of duration model	11. PEER NGA-East Median Ground-Motion Models (J. Hollenbeck, N. Kuehn, C.A. Goulet and N.A. Abrahamson)

1.4.2 Electronic Appendices

A suite of electronic appendices is organized for each chapter. The last section of each chapter lists the electronic appendices associated to that chapter. For Chapters 2 to 11, some of appendices are the output tables from the model as provided by the GMM developers.

1.5 ACKNOWLEDGMENTS

NGA-East, like other NGA projects, has greatly benefitted from strong interactions among junior and senior researchers, practitioners, and end-users. We thank all the participants for their dedication and efforts.

1.6 LIST OF ELECTONIC APPENDICES FOR CHAPTER 1

1A   Selection of representative attenuation models (PDF document)

1B   Finite fault simulations (PDF document)

1B.1   Finite fault simulations, M-scaling Model 1 coefficients for PSA (Excel workbook)

1B.2   Finite fault simulations, M-scaling Model 2 coefficients for PSA (Excel workbook)

1B.3   Finite fault simulations, M-scaling Model 2 coefficients for FAS (Excel workbook)

2 Point-Source Stochastic-Method Simulations of Ground Motions for the PEER NGA-East Project

David M. Boore

U.S. Geological Survey
Menlo Park, California

Abstract

Ground-motions for the PEER NGA-East project were simulated using a stochastic method. The simulated motions are provided for most of the stipulated distances between R_{RUP} of 0 and 1200 km, **M** from 4 to 8, and 25 ground-motion intensity measures: peak ground velocity (PGV), peak ground acceleration (PGA), and 5%-damped pseudo-absolute response spectral acceleration (PSA) from 0.01 sec to 10.0 sec. Tables of motions are provided for each of six attenuation models (Section 1.3.3). The attenuation-model-dependent stress parameters used in the stochastic-method simulations were derived from inversion of PSA data from eight earthquakes in eastern North America (ENA).

2.1   INTRODUCTION

This report describes point-source, stochastic-method simulations of ground motions for ground-motion intensity measures (GMIMs), moment magnitudes (**M**), and rupture distances specified by the Management Team of the NGA-East project. The simulations are for a site for which $V_{S30} = 3.0 \, \text{km/sec}$. The Management Team specified the attenuation models (geometric spreading and Q) to be used, but I chose the other parameters needed in the simulations: (1) I describe the simulation method and the parameters used in the simulations (in particular, the stress parameter for each attenuation model, the finite-fault (FF) factor used to convert from R_{RUP} to the effective point-source distance R_{PS}, the path duration, and the crustal amplifications, as well as the average radiation pattern and the velocity and density in the source region); (2) I show the results of the simulations [the results are in the form of tables of motion, not ground-motion prediction equations [GMPEs]); and (3) I conclude with some comments about the range of applicability of the motions and limitations of the simulations.

2.2 SIMULATION METHOD

The point-source (PS) stochastic method for simulating earthquake ground motions is well known and will not be discussed here (see Boore [2003] for more information, and Boore and Thompson [2015] [BT15] for some recent revisions to the method as implemented in the SMSIM suite of programs [Boore 2005]). What will be discussed here are the parameters to be used in the simulations (a sample file containing the parameters used in the SMSIM simulations is given in Appendix 2A). The parameters fall into several general categories: source, path, and site. The discussions in this section are organized by these categories. Although it is usual to start with the source, I begin the discussion with the path parameters, because the stress parameters of the source are dependent on the path parameters.

The inversions for the stress parameters used my program *stress_param_from_psa*, and the forward simulations used *tmrs_loop_rv_drvr*. These programs use random-vibration simulations with the Der Kiureghian [1980] rms-to-peak factors and the BT15 D_{rms} coefficients. The program *tmrs_loop_rv_drvr* is part of my SMSIM suite of programs, available from the online software page of *www.daveboore.com* [Boore 2005]. The version of SMSIM used for the simulations in this chapter is dated October 15, 2014.

2.2.1 Path Parameters

***Attenuation Models*:**

Six attenuation models (by which I mean a specification of the distance-dependent geometric spreading and the frequency-dependent Q) were provided by the Management Team and are described in Section 1.3.3 and Appendix 1A. These models are summarized in Table 2.1 for convenience. Two of the models (A04 and AB14) are characterized by a geometrical spreading of $1/R^{1.3}$ within the first 70 km and 50 km, respectively, whereas most of the other models have a decay of $1/R$ for these distance ranges. The simplest model is BCA10D, which has $1/R$ geometrical spreading at all distances. As I will show, the difference in the geometrical spreading functions has a large impact on the stress parameters derived from data, as well as the ability to fit the data at a wide range of periods. It is important to note that I am not endorsing any of the models, although I find that the best overall model is BS11, closely followed by the BCA10D and AB95 models; the two models with $1/R^{1.3}$ geometrical spreading cannot fit the data at periods of 1 sec and 2 sec, no matter what stress parameter is used.

***Path-Dependent Durations*:**

One of the main changes relative to parameters used in my previous simulations for ground motions in ENA is the path duration, as shown in Figure 2.1. Details regarding the derivation of the new durations are in Boore and Thompson [2015]. The much longer durations than those used before (the previous durations are shown by the gray line in Figure 2.1) will result in lower ground motions for a given stress parameter and attenuation model; therefore, I needed to determine the stress parameter to be used for each attenuation model—I cannot simply use the stress parameters in Boore [2012]. The duration function is given in Table 2.2.

Table 2.1   Summary of attenuation models from Section 1.3.3.

Model	Geometrical spreading*	Q	Reference
A04	-1.3(70)0.2(140)-0.5	$\max(1000, 893\,f^{\,0.32})$	Atkinson [2004]
AB14	-1.3(50)-0.5	$525\,f^{\,0.45}$	Atkinson and Boore [2014]
AB95	-1.0(70)0.0(130)-0.5	$680\,f^{\,0.36}$	Atkinson and Boore [1995]
BCA10D	-1.0	2850	Boore et al. [2010]
BS11	-1.0(50)-0.5	$410\,f^{\,0.5}$	Boatwright and Seekins [2011]
SGD02	-1.1(80)-0.55	$351\,f^{\,0.84}$	Silva et al. [2002]

* The entries are shorthand for the geometrical spreading function; the numbers in parenthesis are the breakpoint distances, with the exponent of R being given by the numbers on either side of the breakpoint distance. Note that the AB14 geometrical spreading is frequency dependent--the function shown is for frequencies of 5 Hz and above; for lower frequencies the equivalent power is negative with an absolute value greater than 1.3 for distances within 50 km, except at distances less than about 10 km. The SGD02 model is magnitude dependent; the coefficients given in the table are for **M**=5.

Table 2.2   The path duration model for stable continental regions[*] (from Boore and Thompson [2015]).

R_{PS} **(km)**	D_P **(sec)**
0.0	0.0
15.0	2.6
35.0	17.5
50.0	25.1
125.0	25.1
200.0	28.5
392.0	46.0
600.0	69.1
Slope of last segment	0.111

[*]Values for non-tabulated distances are given by linear interpolation of the tabulated values (in terms of duration and distance, not logarithms of these quantities). Durations for distance beyond the last tabulated distance are given by

$$D_P(R) = D_P(R_{last}) + slope \times (R - R_{last}).$$
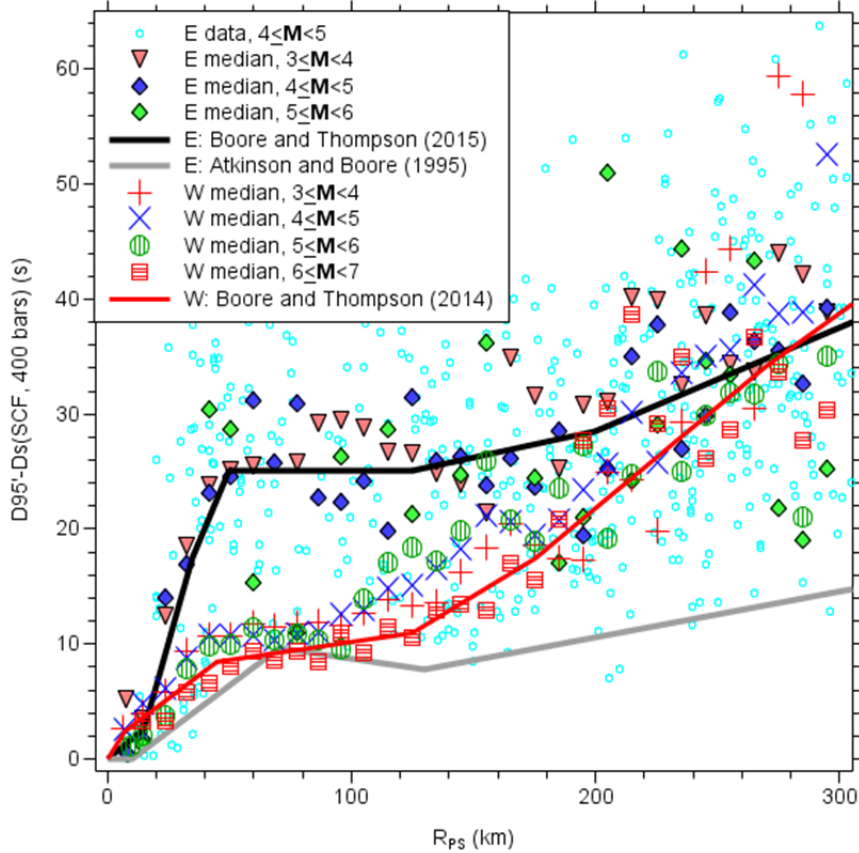
Figure 2.1 The medians in various magnitude (**M**) and point-source distance (R_{PS}) bins of the path duration $D_P = D'_{95} - D_S$ for data both from ENA ("E") and active crustal regions (ACRs) ("W"). The source duration D_S is given by $1/f_c$, in which the corner frequency f_c is given by the single-corner frequency model with a stress parameter of 400 bars. Guided primarily by the medians for the **M** = 4 to 5 range (the individual data points for this magnitude range are shown by the small open circles), Boore and Thompson [2015] subjectively derived a path duration function consisting of joined linear segments. For comparison, D_P used in some previous simulations of motions in ENA [Atkinson and Boore 1995] and the recent path duration for ACRs [Boore and Thompson 2014] are also shown. Modified from Boore and Thompson [2015], which should be consulted for more details.

Crustal Amplification:

Two crustal amplification models were used in the simulations, one for the final simulations, for which it was stipulated that the velocity model had $V_{S30} = 3.0$ km/sec [Hashash et al. 2014a, b] and one with $V_{S30} = 2.0$ km/sec for the inversion of data for the stress parameters to be used in the final simulations. Table 2.3 contains the amplifications. The data used in the inversions were

intended to be from hard rock sites, but according to the NGA-East flatfile, the V_{S30} at the sites is probably closer to 2.0 km/sec than 3.0 km/sec. The two amplifications are shown in Figure 2.2, which also shows the effect of applying a diminution operator $\exp(-\pi\kappa f)$ with $\kappa = 0.006\,\text{sec}$. The amplifications were computed using the square-root-impedance method [Boore 2013], assuming a source density of 2.8 *g*/cc and a shear-wave velocity of 3.7 km/sec, a vertical angle of incidence, and no attenuation (see BT15). The velocity profiles used in the amplification calculations are based on the very hard rock profile of Boore and Joyner [1997] (BJ97). For $V_{S30} = 3000\,\text{m/sec}$, the top 300 m of the Boore and Joyner profile was replaced by a layer with a velocity of 3000 m/sec (see BT15). The profile for which $V_{S30} = 2000\,\text{m/sec}$ was constructed by replacing the top 300 m of the standard hard rock profile of BJ97 with a 30-m-thick layer with a constant velocity of 2000 m/sec, underlain by material with a linear gradient that connected the 2000 m/sec value at 30 m with the 3000 m/sec value at a depth of 300 m in the BJ97 very hard rock profile. More information can be found in Boore [2015].

Table 2.3 Crustal amplification (A) and frequency (f) pairs for stable continental regions (SCRs) for velocity models for which and $V_{S30} = 3.0$ km/sec (the latter modified from Table 4 in Boore and Joyner [1997][*].

f	$A(V_{S30} = 2.0$ km/sec$)$	f	$A(V_{S30} = 3.0$ km/sec$)$
0.010	1.000	0.001	1.000
0.015	1.008	0.008	1.003
0.032	1.015	0.023	1.010
0.054	1.026	0.040	1.017
0.078	1.038	0.061	1.026
0.111	1.055	0.108	1.047
0.168	1.069	0.234	1.069
0.245	1.086	0.345	1.084
0.387	1.116	0.508	1.101
0.647	1.159	1.090	1.135
0.950	1.202	1.370	1.143
1.556	1.270	1.690	1.148
2.333	1.342	1.970	1.150
3.156	1.386	2.420	1.151
4.333	1.420	—	—
6.126	1.445	—	—
8.662	1.461	—	—
11.376	1.467	—	—
15.164	1.471	—	—
25.586	1.471	—	—

[*]Values for non-tabulated frequencies are given by linear interpolation of the logarithms of the tabulated values. Amplifications for frequencies less than and greater than the tabulated frequencies take on the values at the closest tabulated frequencies.
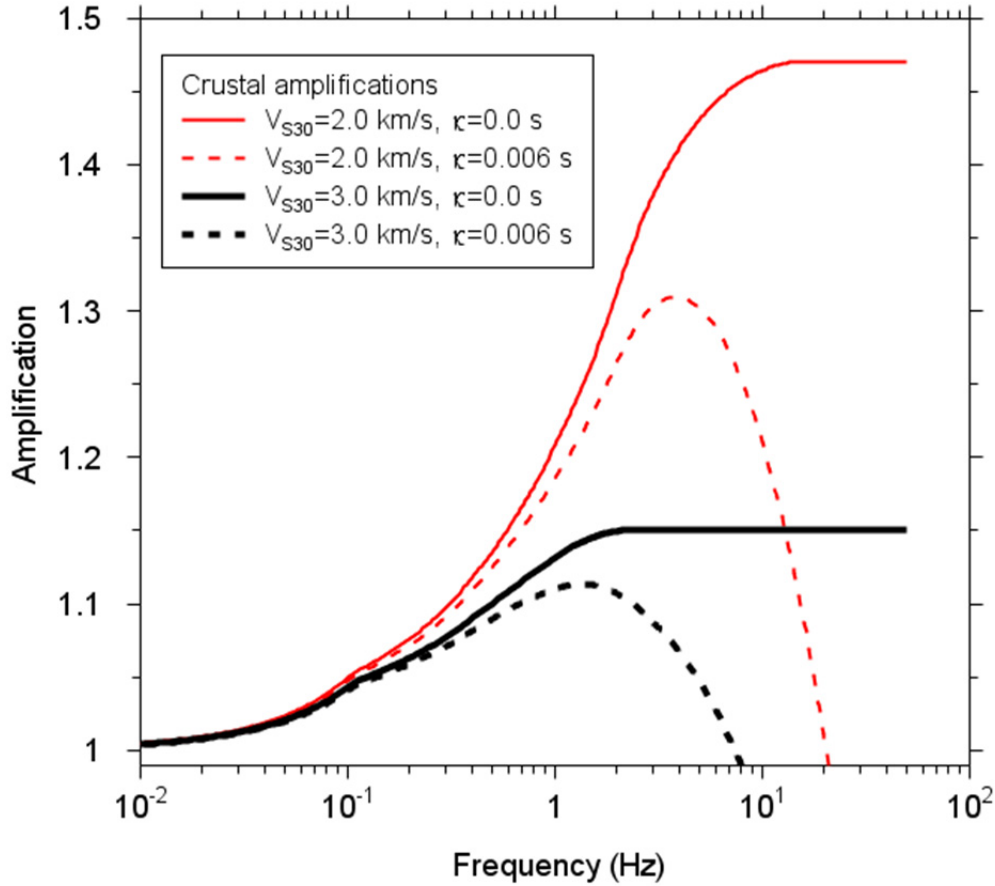
Figure 2.2   Crustal amplifications for sites with two values of V_{S30}: 2.0 km/sec and 3.0 km/sec. Shown are the amplifications without attenuation (solid curves) and with attenuation, as modeled by the diminution operator $\exp(-\pi \kappa f)$, where $\kappa = 0.006 \sec$. See Boore and Thompson [2015] for more details.

Diminution Parameter κ:

The stipulated value of 0.006 sec [Campbell et al. 2014] was used in the simulations.

2.3   SOURCE PROPERTIES

The properties that need to be specified are the spectral shape of the source and how it changes with magnitude, the average radiation pattern, and the adjustment of distance to account for the finite size of the source.

Average Radiation Pattern and Density, and Shear-Wave Velocity near the Source:

The simulations used a value of 55 for the average radiation pattern (e.g., Boore and Boatwright [1984]), and a shear-wave velocity and density in the source region of 3.7 km/sec and 2.8 *g*/cc. These primarily enter into the simulations as part of a frequency-independent constant, and

because these parameters were used in the inversion of data for the stress parameters and then in forward calculations using the stress parameters, the effect of any changes in the average radiation pattern or source velocity or density would be canceled out.

Source Spectral Shape:

I used a single-corner frequency (SCF), constant stress parameter model. Using a more general, double-corner frequency model (e.g., Boore et al. [2014]) would require choosing the values of more parameters. There are barely sufficient data to estimate the single stress parameter $(\Delta\sigma)$ needed in the SCF model, however, and for that reason I used the SCF model.

Finite-Fault Adjustment to Distance:

The ground-motion predictions used in hazard calculations usually use the closest distance to the rupture surface (R_{RUP}) as the distance metric in the calculations. As discussed in detail in BT15, however, the distance to be used in point-source stochastic method simulations should be R_{PS}, where

$$R_{PS} = \sqrt{R_{RUP}^2 + h(\mathbf{M})^2} \tag{2.1}$$

and $h(\mathbf{M})$ is a factor that accounts for the finiteness of the rupture surface of a fault. In this study, I use the equations of BT15 for $h(\mathbf{M})$; these are a combination of the relations of Yenier and Atkinson [2014; 2015a]. The relations are shown in Figure 2.3 as a function of magnitude.

Stress Parameter:

For a given attenuation model, the most important parameter that must be specified is the stress parameter $\Delta\sigma$. To obtain a feeling for the stress parameters needed to fit data for each of the attenuation models, as well as to judge the ability of the models to fit data over a range of distances and periods, Figures 2.4–2.9 compare the data from the Riviere du Loup earthquake with simulations for a wide range of stress parameters (centered at 800 bars) for oscillator periods of 0.1, 0.2, 1.0, and 2.0 sec, $V_{S30} = 2.0$ km/sec, and the six models of attenuation. Careful inspection of these figures leads to these conclusions:

1. The two models that have $1/R^{1.3}$ within the first 70 to 50 km (A04 and AB14; Figures 4 and 5) require a large value of the stress parameter to match the response spectral observations at $T = 0.1$ sec and $T = 0.2$ sec; no values of the stress parameter will allow the simulations to match the observations at periods of 1.0 sec and 2.0 sec.

2. At short periods and for most of the attenuation models, the stress parameter that leads to the best match of the data for distances within about 200 km leads to an overestimation of the data at greater distances. The one clear exception to this is the BS11 model. This is subjectively the best of the six models in terms of its ability to match data at a wide range of distances and periods.

3. The simplest model (BCA10D), with $1/R$ spreading at all distances, can match the data for a wide range of periods for distances less than about 400 km, but unlike the BS11 model, it seems to require different stress parameters to match the short-period data at different distances.

4. Both the BS11 and the BCA10D models underestimate the bulk of the longer-period data beyond about 400 km, no matter what stress parameter is used.

Similar conclusions can be drawn from similar comparisons for the Saguenay and Val des Bois earthquakes (figures comparable to Figures 2.4–2.9 for those earthquakes are not shown here because of space limitations).

With this background in the ability of the six attenuation models to match the data, I inverted the data of Boore (2012) for $\Delta\sigma$, using the SMSIM parameters previously discussed (Appendix 2A shows one of the SMSIM parameter files used in the analysis). I followed the methodology of Boore et al. [2010], for each attenuation model. I did separate inversions for the data within 200 km and within 600 km. The results are in Table 2.4–Table 2.9 (one table for each attenuation model; all tables have the same format). In those tables I also include the geometric means and the factor corresponding to 10 raised to the power of the standard deviation of the log mean of the stress parameters. The individual stress parameters as well as the geometric means are shown in Figure 2.10 for the six attenuation models. I used the geometric means obtained from the inversions of data within 200 km for the simulations of ground motions for the NGA-East project, as I felt that it is more important in applications to match the data at closer than at greater distances. The geometric means used in the simulations excluded the stress parameters from the Saguenay earthquake. The main reason for doing this was that the stress parameter from that earthquake is quite high and seems to be an outlier, rather than being part of a normal distribution of $\ln\Delta\sigma$. On the other hand, the stress parameter from the Nahanni earthquake also seems to be a low outlier, at least for some of the attenuation models. In retrospect I should have included the stress parameter for the Saguenay earthquake, and more importantly, because the number of events is so small I should have used the median of the stress parameters for each attenuation model rather than the geometric mean, which equals the median of $\Delta\sigma$ only if $\Delta\sigma$ is log normally distributed. For the BS11 attenuation model, the median stress parameter for all earthquakes inverted from data within 200 km is 172 bars, compared with the 185 bars used in the simulations. I compared the simulations for these two stress parameters for all GMIMs and a subset of magnitudes from 5 to 8 and distances from 10 to 1000 km. The motions for the lower stress parameter are always lower than for the higher stress parameter, but by no more than 5%. This is much less than any reasonable estimate of either aleatory or epistemic uncertainty, and therefore I judge that no changes need to be made in my reported ground motions.
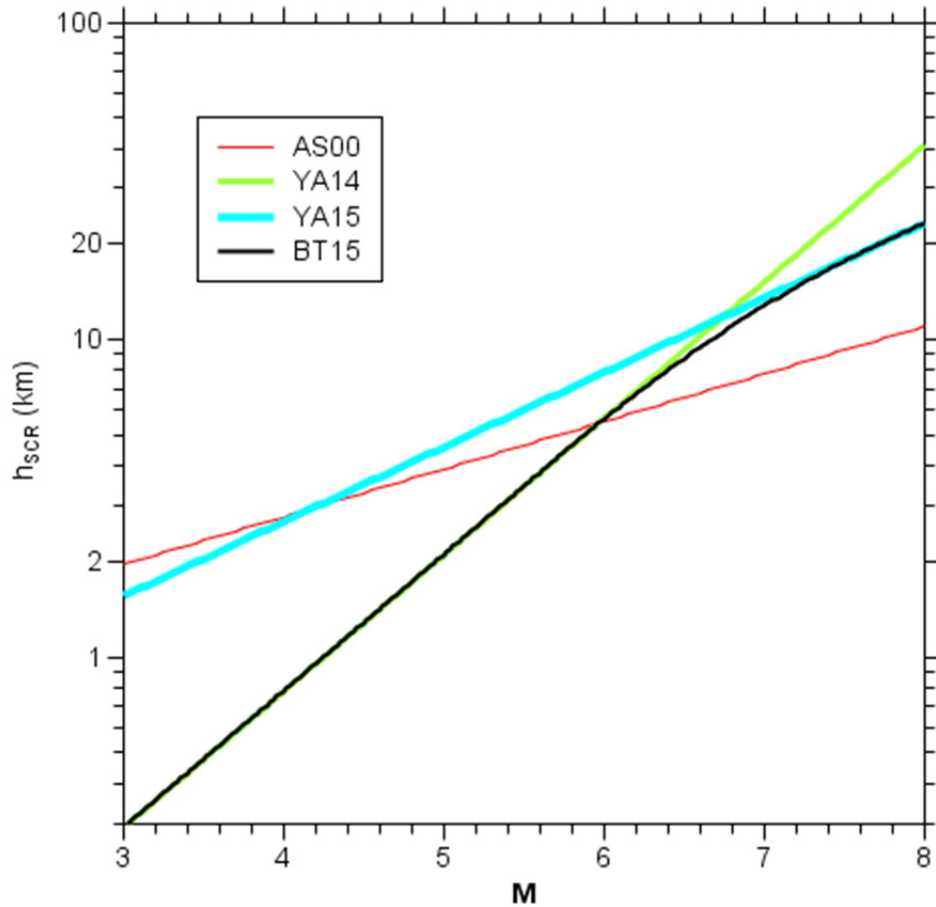
Figure 2.3   The finite-fault (FF) factor h_{SCR} (where "SCR" stands for "stable continental region") used in converting the closest distance to the rupture surface $\left(R_{RUP} \right)$ to the distance to be used in the point-source calculations $\left(R_{PS} \right)$ Shown are the h_{SCR} functions for Atkinson and Silva [2000] (AS00), Yenier and Atkinson [2014] (YA14), Yenier and Atkinson [2015a] (YA15), and Boore and Thompson [2015] (BT15). The FF factors for AS00, YA14, and YA15 are intended for use in ACRs; they have been reduced by a factor of 0.68 to account for the likely higher stress drops for earthquakes in SCRs than in ACRs. Modified from BT15, which should be consulted for more details.
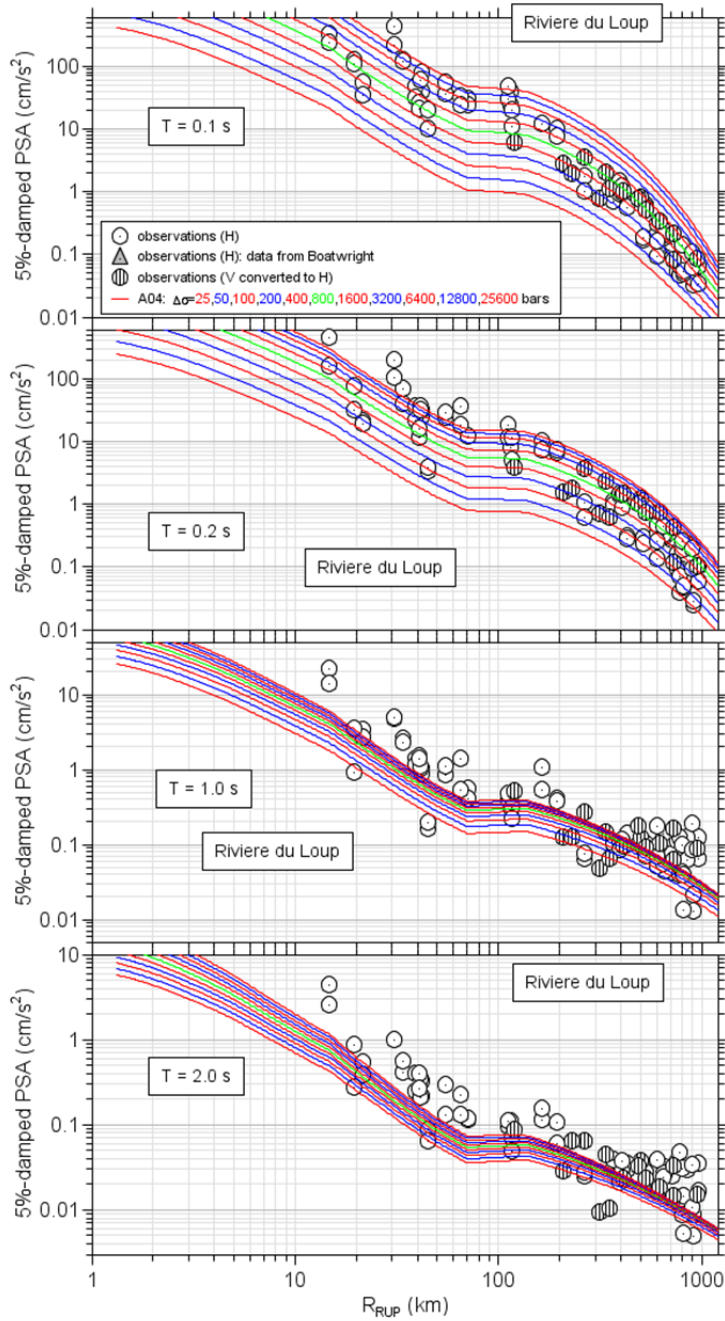
Figure 2.4   Observations from the 2005 Riviere du Loup earthquake (symbols) and
simulated PSA for a suite of stress parameters, using crustal
amplifications for $V_{S30} = 2.0$ km/sec and the Atkinson [2004] (A04)
attenuation model. See Boore [2012] for details regarding the
observations.
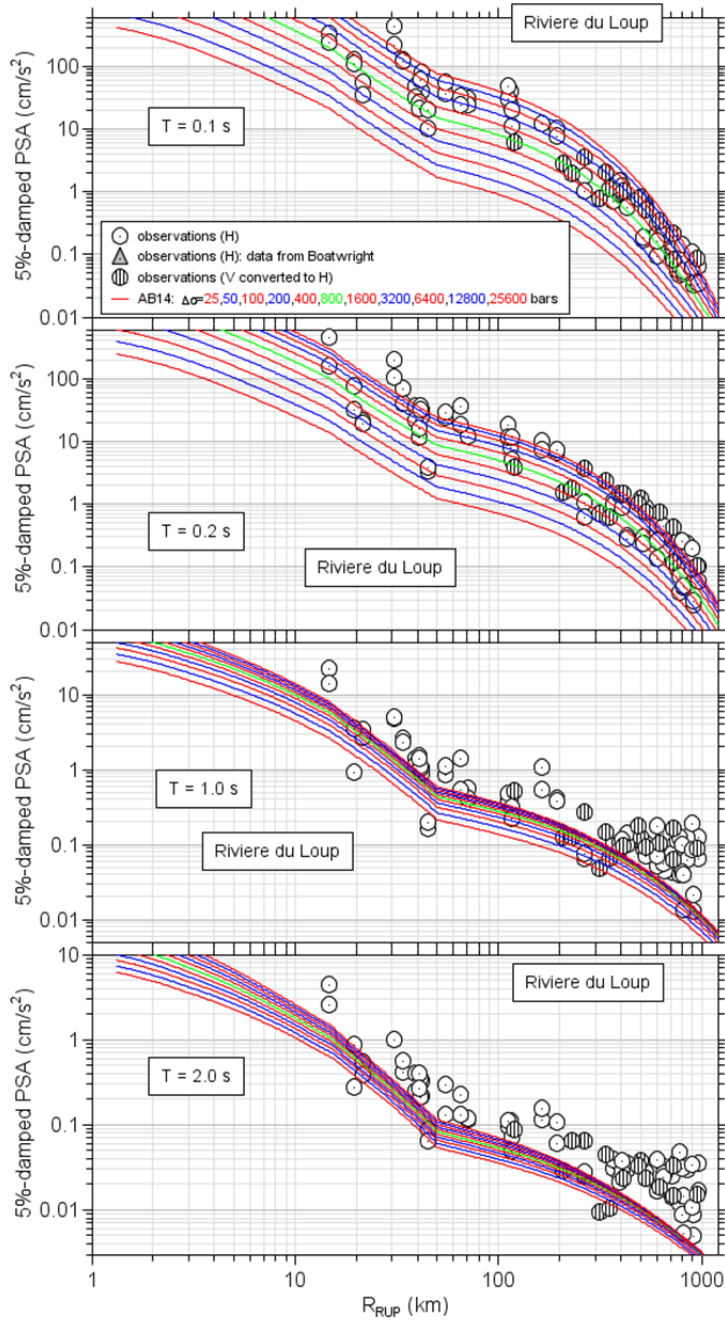
Figure 2.5 Observations from the 2005 Riviere du Loup earthquake (symbols) and simulated PSA for a suite of stress parameters, using crustal amplifications for $V_{S30} = 2.0$ km/sec and the Atkinson and Boore [2014] (AB14) attenuation model. See Boore [2012] for details regarding the observations.
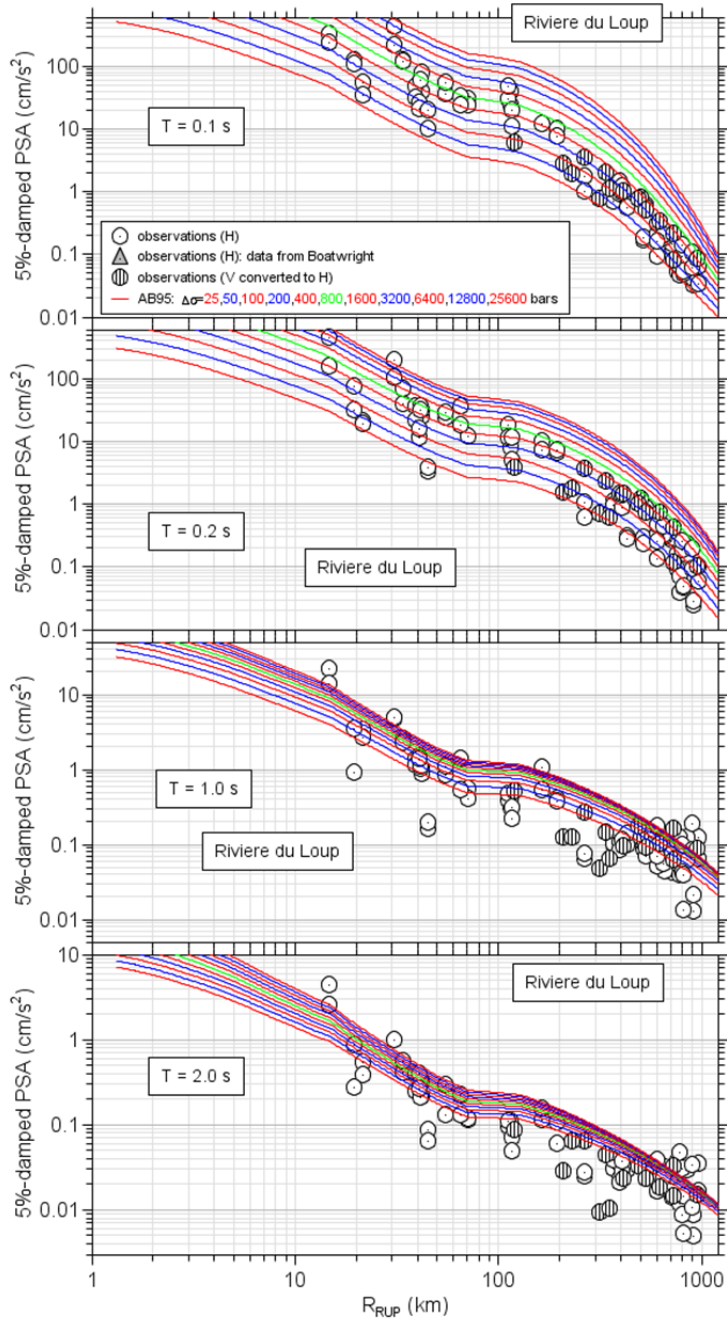
Figure 2.6   Observations from the 2005 Riviere du Loup earthquake (symbols) and simulated PSA for a suite of stress parameters, using crustal amplifications for $V_{S30} = 2.0$ km/sec and the Atkinson and Boore [1995] (AB95) attenuation model. See Boore [2012] for details regarding the observations.
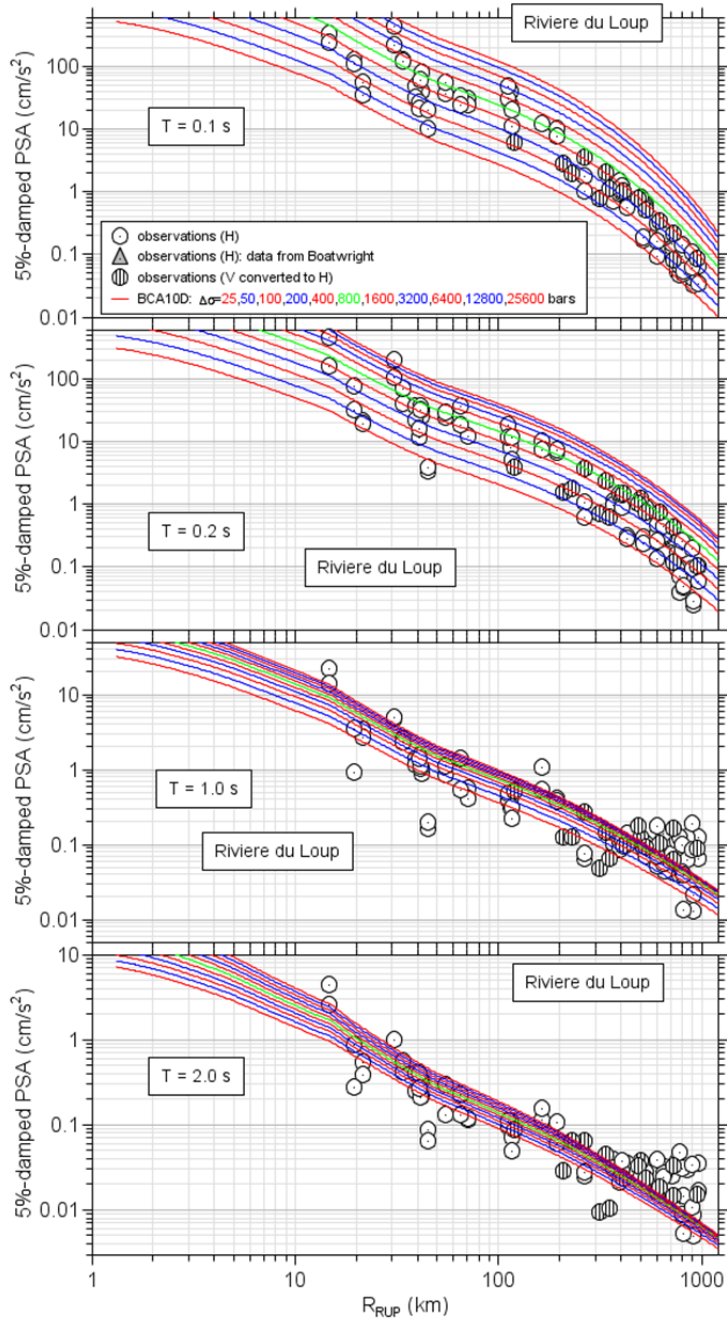
Figure 2.7   Observations from the 2005 Riviere du Loup earthquake (symbols) and simulated PSA for a suite of stress parameters, using crustal amplifications for $V_{S30} = 2.0$ km/sec and the Boore et al. [2010] (BCA10D) attenuation model. See Boore [2012] for details regarding the observations.
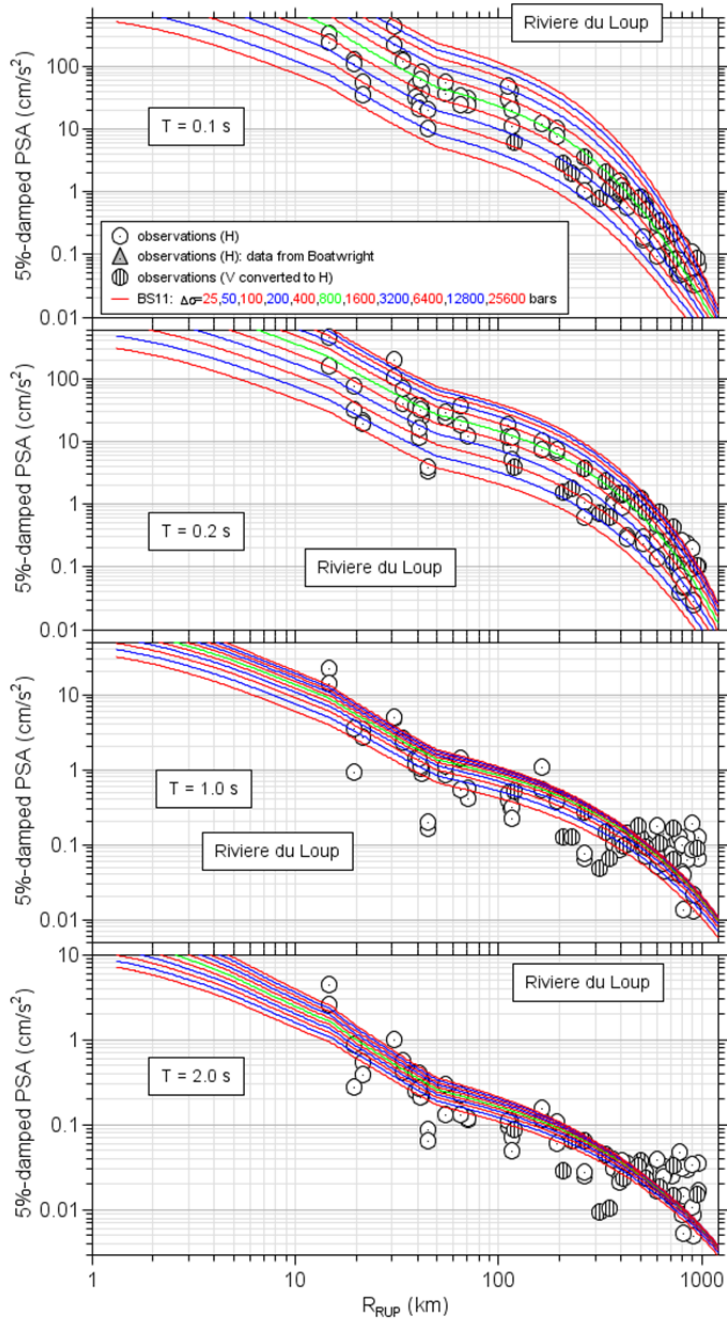
Figure 2.8   Observations from the 2005 Riviere du Loup earthquake (symbols) and simulated PSA for a suite of stress parameters, using crustal amplifications for $V_{S30} = 2.0$ km/sec and the Boatwright and Seekins [2011] (BS11) attenuation model. See Boore [2012] for details regarding the observations.
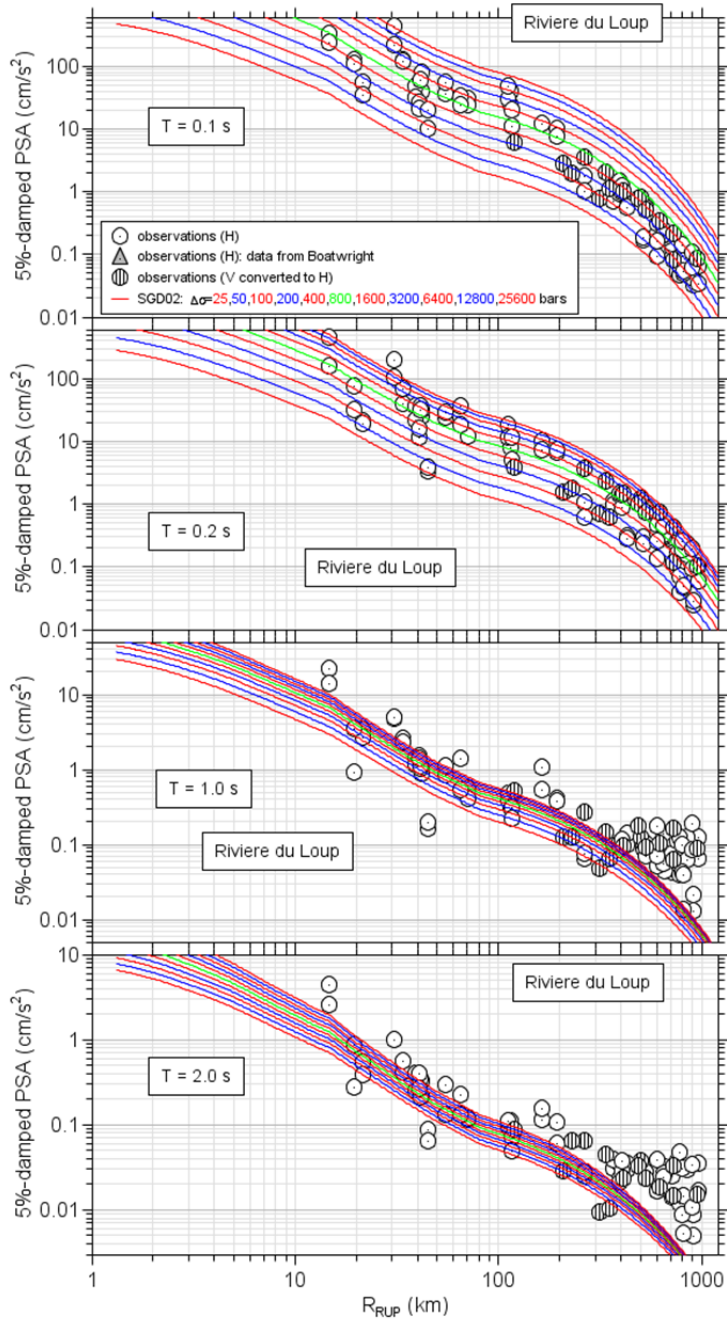
Figure 2.9 Observations from the 2005 Riviere du Loup earthquake (symbols) and simulated PSA for a suite of stress parameters, using crustal amplifications for V_{S30} = 2000 m/sec and the Silva et al. [2002] (SGD02) attenuation model. See Boore [2012] for details regarding the observations.
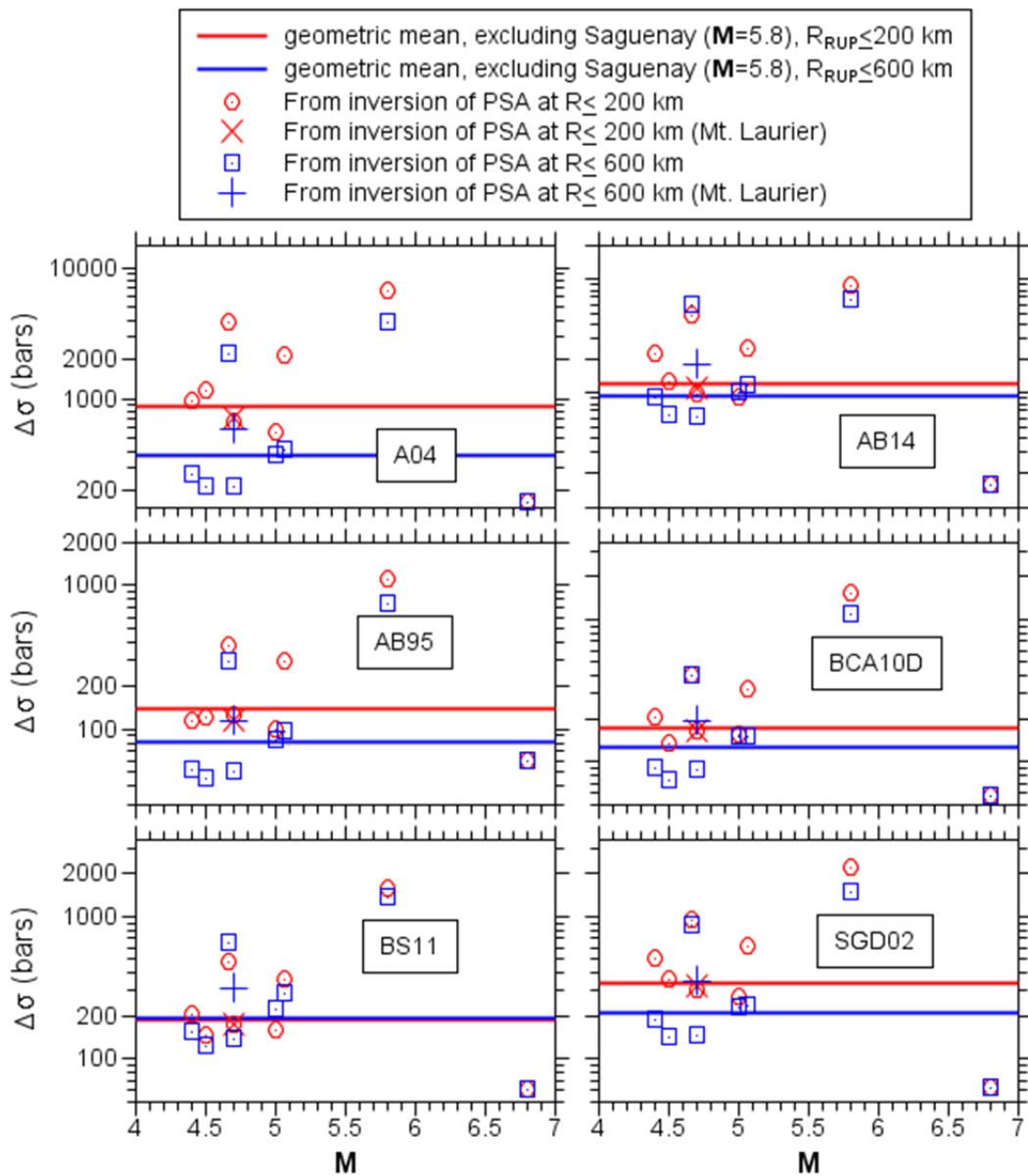
Figure 2.10 Summary of stress parameters obtained from inversions of observed PSA for the six attenuation models. The results from inversions using data within 200 km and within 600 km are shown separately. The stress parameters from recording of the Mt. Laurier earthquake are shown as separate symbols to distinguish those results from the other event (Kipawa) with the same **M**.

Table 2.4 Stress parameters from inverting the 0.1 sec and 0.2 sec PSA from recordings of the indicated events, using the Atkinson [2004] (A04) attenuation model. Two sets of data were used, for maximum distances of 200 km and 600 km. The geometric mean (*gmean*) was computed from the inverted stress parameters, excluding the stress parameter from the Saguenay earthquake; *sdevfctr* is the standard deviation of the mean log stress, expressed as a factor (i.e., 10 raised to the power given by the standard deviation of the mean log stress).

Event	Date (M/D/Y)	M	Attenuation model	Stress (bars) $\left(R_{RUP} < 200\ \mathrm{km} \right)\left(F_M \right)\left(F_Z \right) T\left(\sec \right) \mathbf{M}_h \Delta\sigma$	Stress (bars) $\left(R_{RUP} < 600\ \mathrm{km} \right)$
Nahanni	12/23/1985	6.80	a04	162	162
Saguenay	11/25/1988	5.80	a04	6565	3818
Mt. Laurier	10/19/1990	4.70	a04	703	597
Cap Rouge	11/06/1997	4.41	a04	961	265
St. Anne	03/16/1999	4.50	a04	1155	214
Kipawa	01/01/2000	4.70	a04	668	217
Ausable	04/20/2002	5.00	a04	547	375
Riviere du Loup	03/06/2005	4.67	a04	3848	2225
Val des Bois	06/23/2010	5.07	a04	2165	404
gmean				887	376
sdevfctr				2.6	2.3

Table 2.5   Stress parameters from inverting the 0.1sec and 0.2 sec PSA from recordings of the indicated events, using the Atkinson and Boore [2014] (AB14) attenuation model. Two sets of data were used, for maximum distances of 200 km and 600 km. The geometric mean (*gmean*) was computed from the inverted stress parameters, excluding the stress parameter from the Saguenay earthquake; *sdevfctr* is the standard deviation of the mean log stress, expressed as a factor (i.e., 10 raised to the power given by the standard deviation of the mean log stress).

Event	Date (M/D/Y)	M	Attenuation model	Stress (bars) $\left(R_{RUP} < 200 \text{ km} \right)$	Stress (bars) $\left(R_{RUP} < 600 \text{ km} \right)$
Nahanni	12/23/1985	6.80	ab14	157	157
Saguenay	11/25/1988	5.80	ab14	8720	6559
Mt. Laurier	10/19/1990	4.70	ab14	1100	1811
Cap Rouge	11/06/1997	4.41	ab14	2206	923
St. Anne	03/16/1999	4.50	ab14	1236	635
Kipawa	01/01/2000	4.70	ab14	989	625
Ausable	04/20/2002	5.00	ab14	896	1001
Riviere du Loup	03/06/2005	4.67	ab14	4731	5888
Val des Bois	06/23/2010	5.07	ab14	2461	1181
gmean				1219	961
sdevfctr				2.7	2.8

Table 2.6 Stress parameters from inverting the 0.1sec and 0.2 sec PSA from recordings of the indicated events, using the Atkinson and Boore [1995] (AB95) attenuation model. Two sets of data were used, for maximum distances of 200 km and 600 km. The geometric mean (*gmean*) was computed from the inverted stress parameters, excluding the stress parameter from the Saguenay earthquake; *sdevfctr* is the standard deviation of the mean log stress, expressed as a factor (i.e., 10 raised to the power given by the standard deviation of the mean log stress).

Event	Date (M/D/Y)	M	Attenuation model	Stress (bars) $\left(R_{RUP} < 200 \text{ km} \right)$	Stress (bars) $\left(R_{RUP} < 600 \text{ km} \right)$
Nahanni	12/23/1985	6.80	ab95	59	59
Saguenay	11/25/1988	5.80	ab95	1109	738
Mt. Laurier	10/19/1990	4.70	ab95	113	115
Cap Rouge	11/06/1997	4.41	ab95	113	52
St. Anne	03/16/1999	4.50	ab95	119	45
Kipawa	01/01/2000	4.70	ab95	124	51
Ausable	04/20/2002	5.00	ab95	98	84
Riviere du Loup	03/06/2005	4.67	ab95	382	296
Val des Bois	06/23/2010	5.07	ab95	296	95
gmean				137	81
sdevfctr				1.8	1.9

Table 2.7   Stress parameters from inverting the 0.1sec and 0.2 sec PSA from recordings of the indicated events, using the Boore et al. [2010] (BCA10D) attenuation model. Two sets of data were used, for maximum distances of 200 km and 600 km. The geometric mean (*gmean*) was computed from the inverted stress parameters, excluding the stress parameter from the Saguenay earthquake; *sdevfctr* is the standard deviation of the mean log stress, expressed as a factor (i.e., 10 raised to the power given by the standard deviation of the mean log stress).

Event	Date (M/D/Y)	M	Attenuation model	Stress (bars) $\left(R_{RUP} < 200 \text{ km} \right)$	Stress (bars) $\left(R_{RUP} < 600 \text{ km} \right)$
Nahanni	12/23/1985	6.80	bca10d	57	57
Saguenay	11/25/1988	5.80	bca10d	1499	1082
Mt. Laurier	10/19/1990	4.70	bca10d	162	193
Cap Rouge	11/06/1997	4.41	bca10d	202	91
St. Anne	03/16/1999	4.50	bca10d	134	74
Kipawa	01/01/2000	4.70	bca10d	162	88
Ausable	04/20/2002	5.00	bca10d	155	150
Riviere du Loup	03/06/2005	4.67	bca10d	405	399
Val des Bois	06/23/2010	5.07	bca10d	319	150
gmean				173	125
sdevfctr				1.8	1.9

Table 2.8   Stress parameters from inverting the 0.1sec and 0.2 sec PSA from recordings of the indicated events, using the Boatwright and Seekins [2011] (BS11) attenuation model. Two sets of data were used, for maximum distances of 200 km and 600 km. The geometric mean (*gmean*) was computed from the inverted stress parameters, excluding the stress parameter from the Saguenay earthquake; *sdevfctr* is the standard deviation of the mean log stress, expressed as a factor (i.e., 10 raised to the power given by the standard deviation of the mean log stress).

Event	Date (M/D/Y)	M	Attenuation model	Stress (bars) $\left(R_{RUP} < 200 \text{ km}\right)$	Stress (bars) $\left(R_{RUP} < 600 \text{ km}\right)$
Nahanni	12/23/1985	6.80	bs11	61	61
Saguenay	11/25/1988	5.80	bs11	1563	1361
Mt. Laurier	10/19/1990	4.70	bs11	170	313
Cap Rouge	11/06/1997	4.41	bs11	202	151
St. Anne	03/16/1999	4.50	bs11	144	123
Kipawa	01/01/2000	4.70	bs11	172	138
Ausable	04/20/2002	5.00	bs11	156	220
Riviere du Loup	03/06/2005	4.67	bs11	472	656
Val des Bois	06/23/2010	5.07	bs11	361	288
gmean				185	194
sdevfctr				1.9	2.1

Table 2.9 Stress parameters from inverting the 0.1sec and 0.2 sec PSA from recordings of the indicated events, using the Silva et al. [2002] (SGD02) attenuation model. Two sets of data were used, for maximum distances of 200 km and 600 km. The geometric mean (*gmean*) was computed from the inverted stress parameters, excluding the stress parameter from the Saguenay earthquake; *sdevfctr* is the standard deviation of the mean log stress, expressed as a factor (i.e., 10 raised to the power given by the standard deviation of the mean log stress).

Event	Date (M/D/Y)	M	Attenuation Model	Stress (bars) $(R_{RUP} < 200 \text{ km})$	Stress (bars) $(R_{RUP} < 600 \text{ km})$
Nahanni	12/23/1985	6.80	sgd02	62	62
Saguenay	11/25/1988	5.80	sgd02	2193	1459
Mt. Laurier	10/19/1990	4.70	sgd02	320	352
Cap Rouge	11/06/1997	4.41	sgd02	511	187
St. Anne	03/16/1999	4.50	sgd02	355	141
Kipawa	01/01/2000	4.70	sgd02	300	146
Ausable	04/20/2002	5.00	sgd02	272	229
Riviere du Loup	03/06/2005	4.67	sgd02	939	851
Val des Bois	06/23/2010	5.07	sgd02	621	233
gmean				338	210
sdevfctr				2.2	2.1

2.4 SIMULATED MOTIONS FOR THE PEER NGA-EAST PROJECT

In addition to the stress parameters just discussed, other parameters used in the simulations included crustal amplifications for sites with $V_{S30} = 3.0 \text{ km/sec}$, as specified by the Management Team, with $\kappa = 0.006 \text{ sec}$, and the BT15 FF factors; other parameters are given in Appendix 2A. The peak motions were obtained from random-vibration theory, using the Der Kiureghian [1980] rms-to-peak factors and the BT15 D_{RMS} equations. The SMSIM program *tmrs_loop_rv_drv*r was used to do the simulations. The results have been aggregated into six workbooks (appendices 2A-2G) comprising 150 tables, each table being for a given attenuation model and a given GMIM (6 models × 25 GMIMs = 150). Plots of 5%-damped PSA versus R_{RUP} are shown in Figures 2.11–2.17 for periods of 0.01 sec, 0.1 sec, 0.2 sec, 1.0 sec, 2.0 sec, 5 sec, and 10 sec. Each figure shows the motions for all attenuation models, with one magnitude per graph in each figure (magnitudes 5, 6, 7, and 8). Note that all of the attenuation models yield similar motions at distances between about 30 km and 200 km for magnitudes near 5 and for periods of 0.1 sec and 0.2 sec; this makes sense since the stress parameters for each attenuation model were chosen to

give a match to data for these distances, magnitude, and periods. At short distances, the steep decay of the A04 and AB14 models yields higher short-period motions than the other models. The larger motions for the SGD02 attenuation model for larger magnitudes is a consequence of the magnitude-dependent geometrical spreading in that model, something that is not a factor in the other models (but because of the effect of the FF factor, there is an apparent magnitude-dependent decay with distance for these other models—see Figures 2.18–22 for examples). The larger motions for the AB14 model at close distances and long periods is due to the period-dependent geometrical spreading in that model. This period dependence is such that the geometrical spreading is more rapid than $1/R^{1.3}$ at distances between about 10 km and 50 km for period of 1 sec and longer.

Direct comparisons of the distance dependence of the motions from the BS11 model for the four magnitudes are shown in Figures 2.18–2.22 for periods of 0.01 sec, 0.1 sec, 0.2 sec, 1.0 sec, and 2.0 sec. As mentioned earlier, notice the apparent magnitude dependence of the distance decay of the motions. This is largely, if not entirely, due to the magnitude-dependent FF factor. Also note that there is some oversaturation of motions at close distances and short periods. This oversaturation is not present using the Yenier and Atkinson [2015a] FF factors, as shown by the dashed curves in the figures. The difference in the motions using the BT15 and the YA15 FF factors is a result of the stronger magnitude dependence of the FF factors at small magnitudes for BT15 than for YA15. (This discussion will be easier to follow with reference to Equation (2.1) and Figure 2.3, realizing that the simulations use R_{PS} and not R_{RUP} when evaluating all distance-dependent components of the stochastic model.) For a fixed R_{RUP} this stronger dependence leads to an apparent negative magnitude scaling, because at short periods the positive magnitude scaling due to the source scaling is not enough to compensate for the effect of the FF factor. At longer periods the source-scaling effect is strong enough to counter the negative scaling due to the FF factor (e.g., compare Figures 2.18 and 2.22).

The period dependence of the simulations is shown in Figure 2.23 for a wide range of magnitudes and distances. The simulated motions vary smoothly with changes in the predictor variables. The strong distance-dependent changes in the shape of the spectra are a result of the stronger attenuation of the motions with distance at short periods than at long periods.

Figure 2.11 A comparison of simulated 5%-damped response spectra from the six attenuation models for a period of 0.01 sec as a function of distance for four magnitudes. The crustal amplifications used in the simulations were for sites with $V_{S30} = 3.0$ km/sec .

Figure 2.12 A comparison of simulated 5%-damped response spectra from the six attenuation models for a period of 0.1 sec as a function of distance for four magnitudes. The crustal amplifications used in the simulations were for sites with $V_{S30} = 3.0$ km/sec.

Figure 2.13   A comparison of simulated 5%-damped response spectra from the six attenuation models for a period of 0.2 sec as a function of distance for four magnitudes. The crustal amplifications used in the simulations were for sites with $V_{S30} = 3.0$ km/sec .
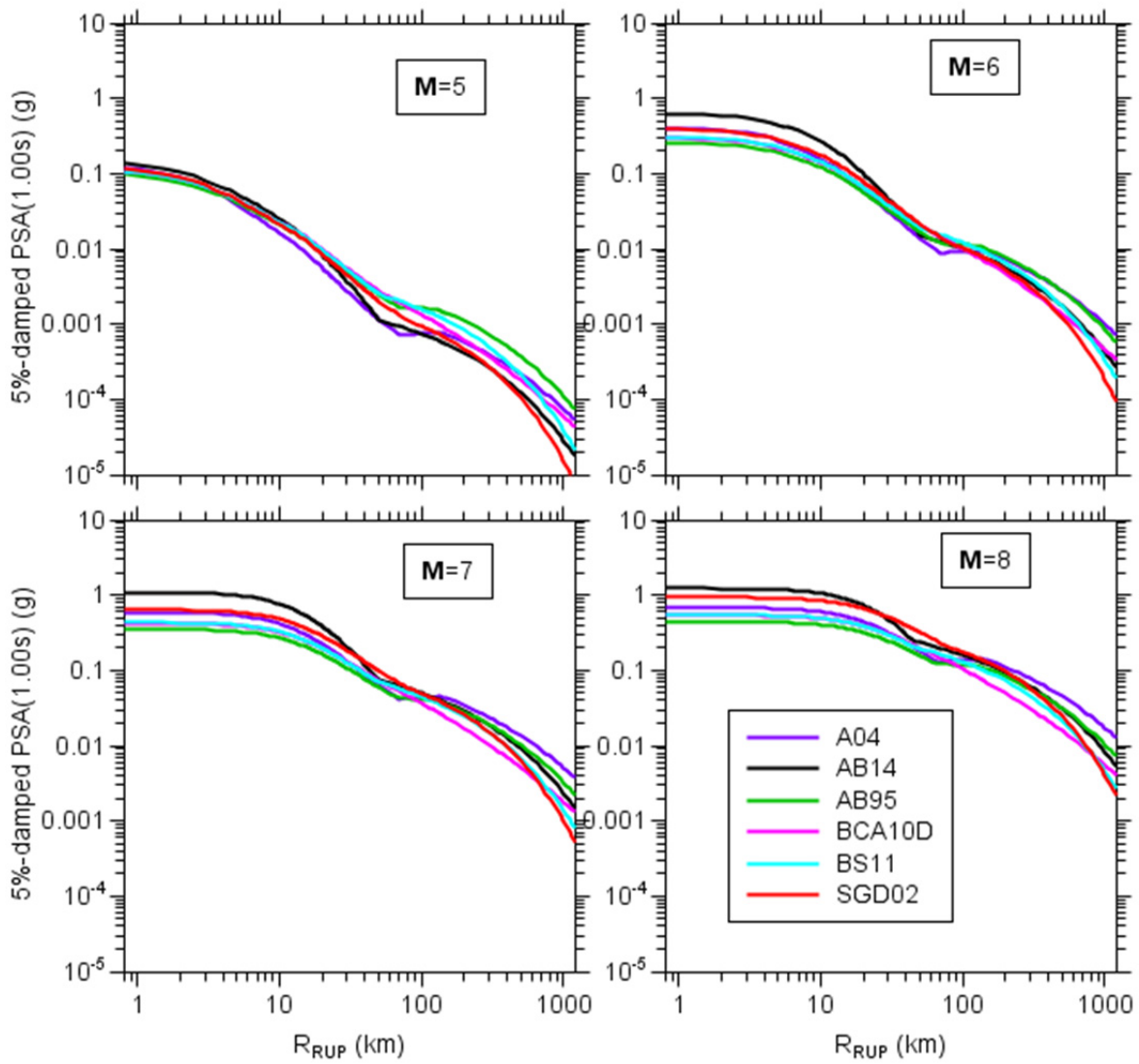
Figure 2.14 A comparison of simulated 5%-damped response spectra from the six attenuation models for a period of 1.0 sec as a function of distance for four magnitudes. The crustal amplifications used in the simulations were for sites with $V_{S30} = 3.0$ km/sec .
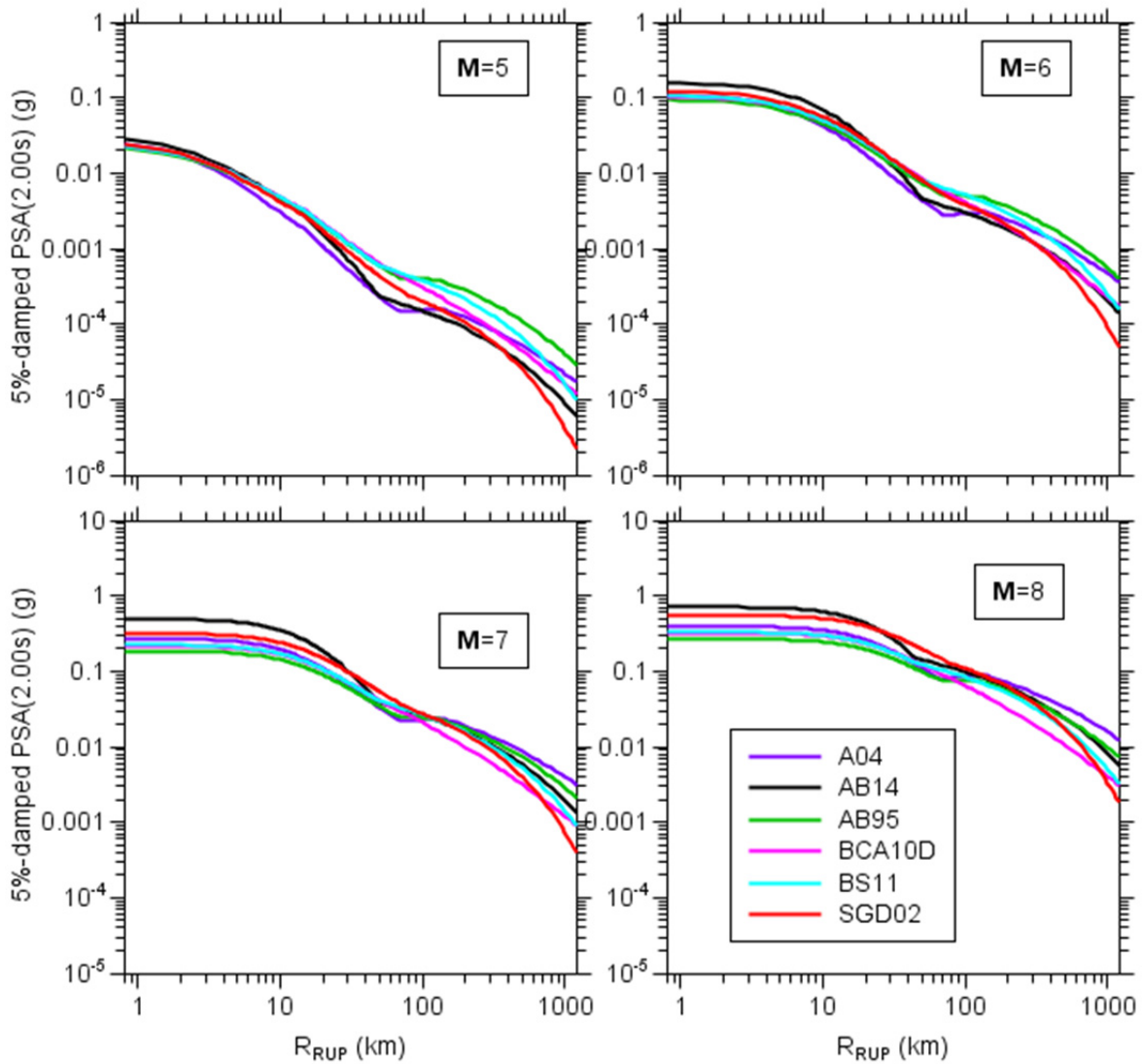
Figure 2.15   A comparison of simulated 5%-damped response spectra from the six attenuation models for a period of 2.0 sec as a function of distance for four magnitudes. The crustal amplifications used in the simulations were for sites with $V_{S30} = 3.0$ km/sec .
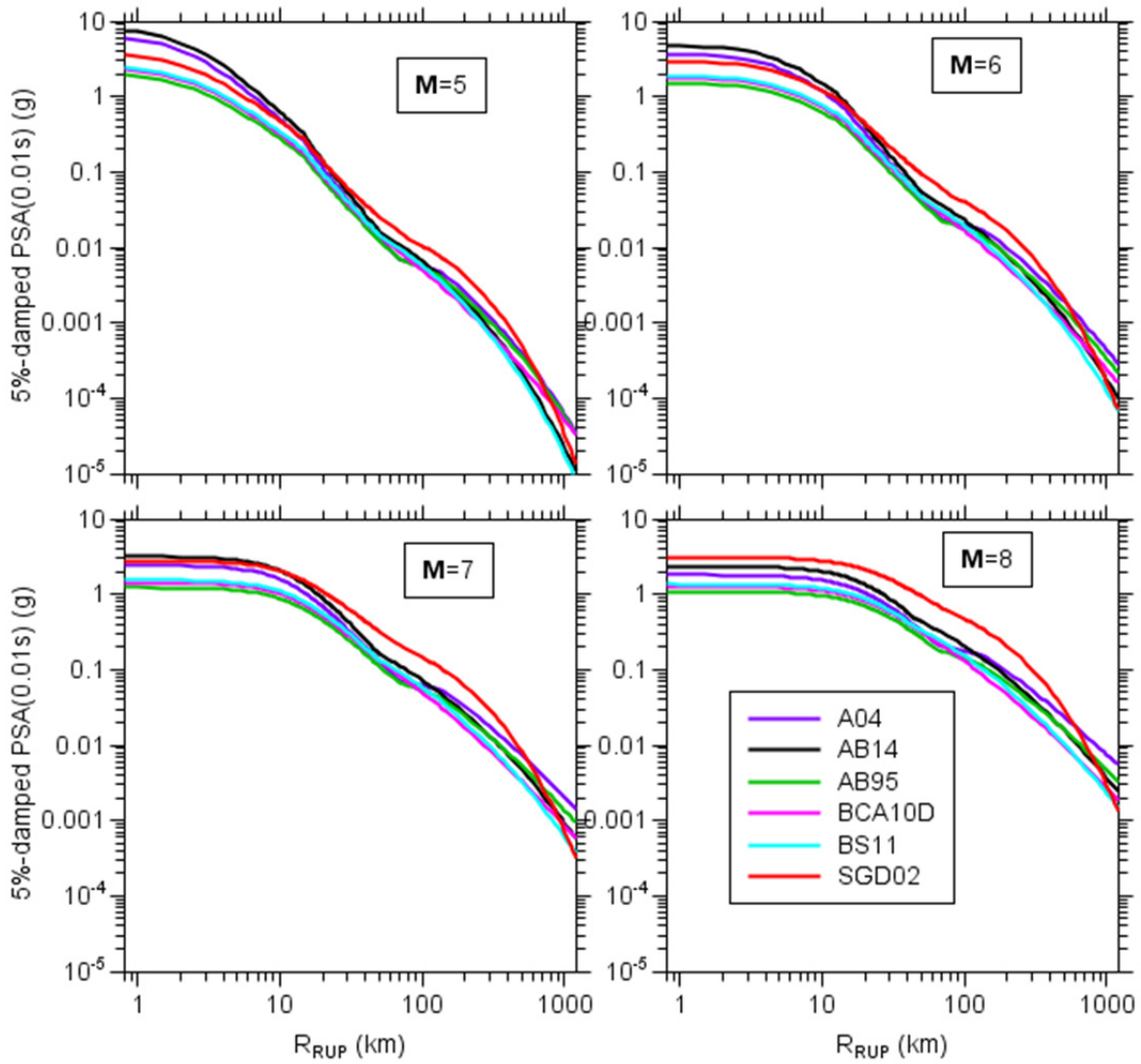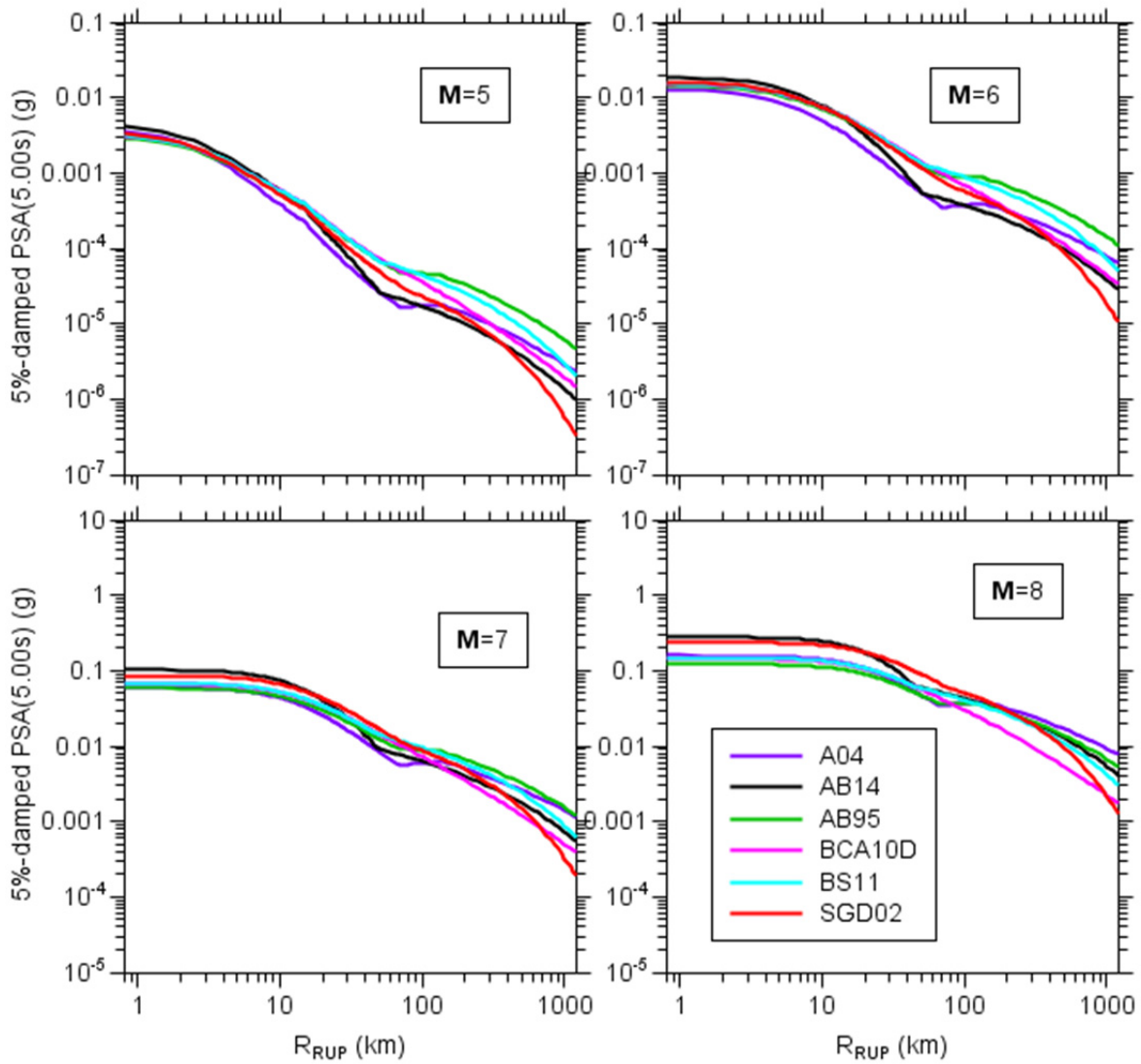
Figure 2.16 A comparison of simulated 5%-damped response spectra from the six attenuation models for a period of 5.0 sec as a function of distance for four magnitudes. The crustal amplifications used in the simulations were for sites with $V_{S30} = 3.0$ km/sec.
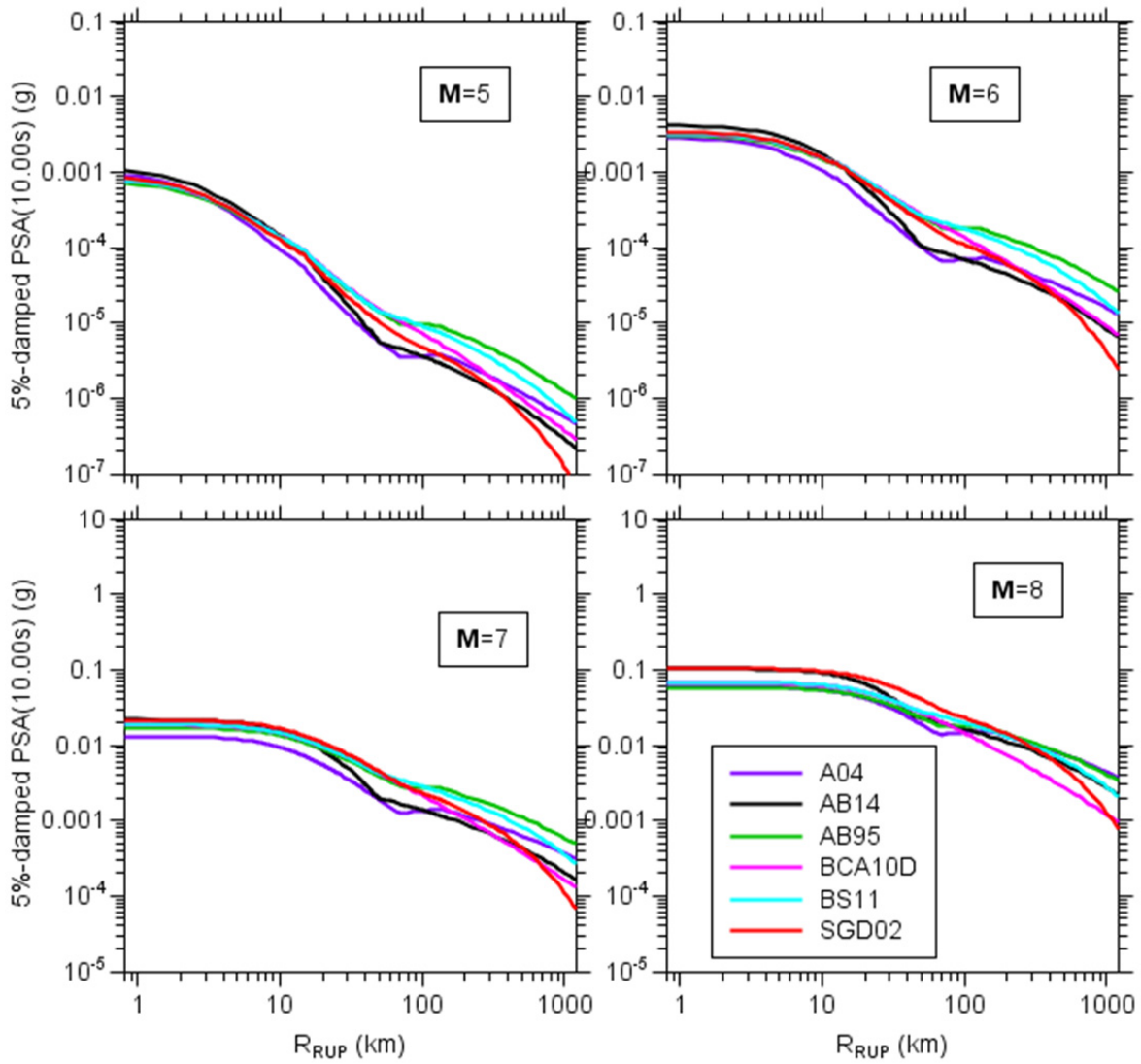
Figure 2.17 A comparison of simulated 5%-damped response spectra from the six attenuation models for a period of 10.0 sec as a function of distance for four magnitudes. The crustal amplifications used in the simulations were for sites with $V_{S30} = 3.0$ km/sec .
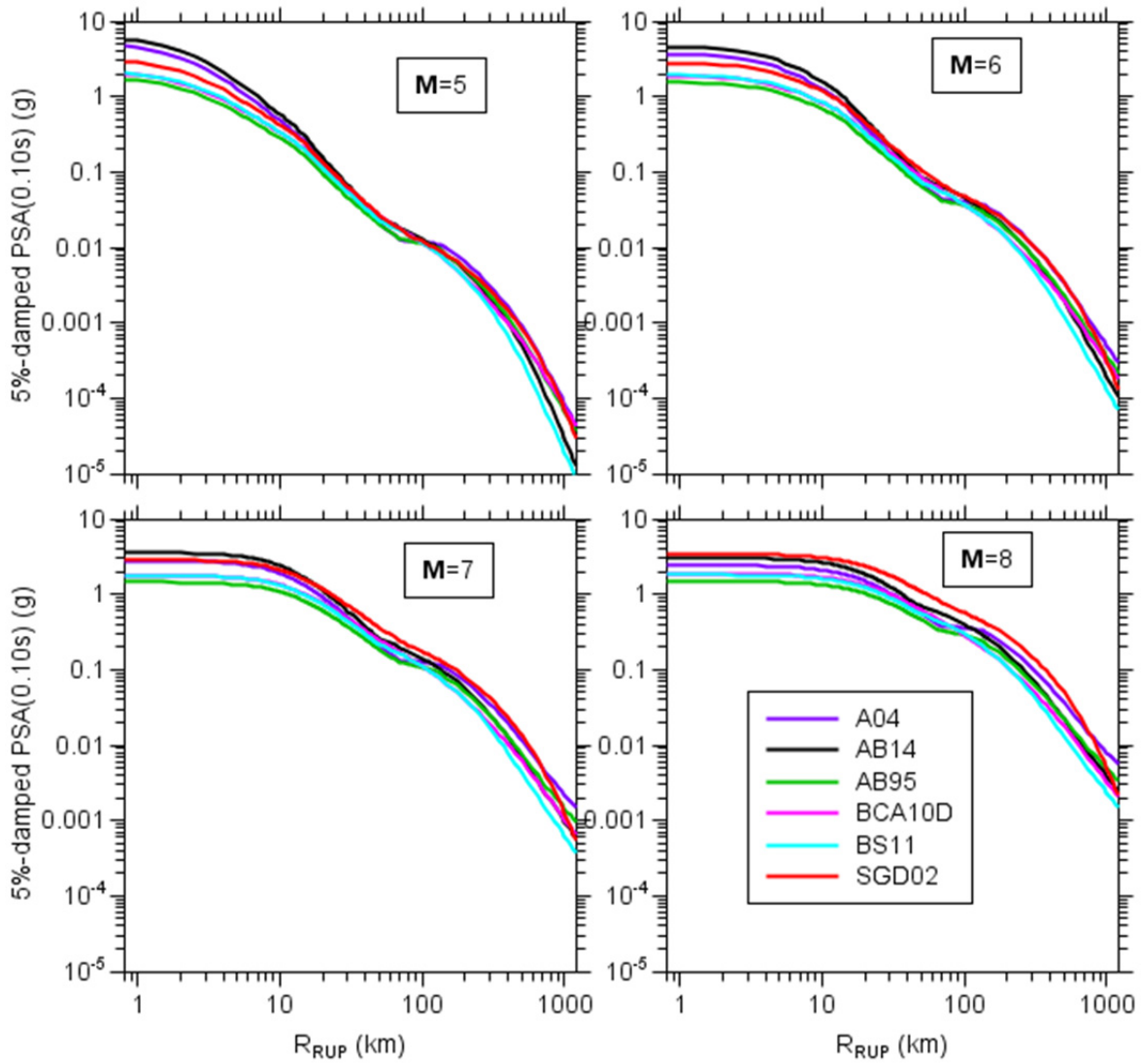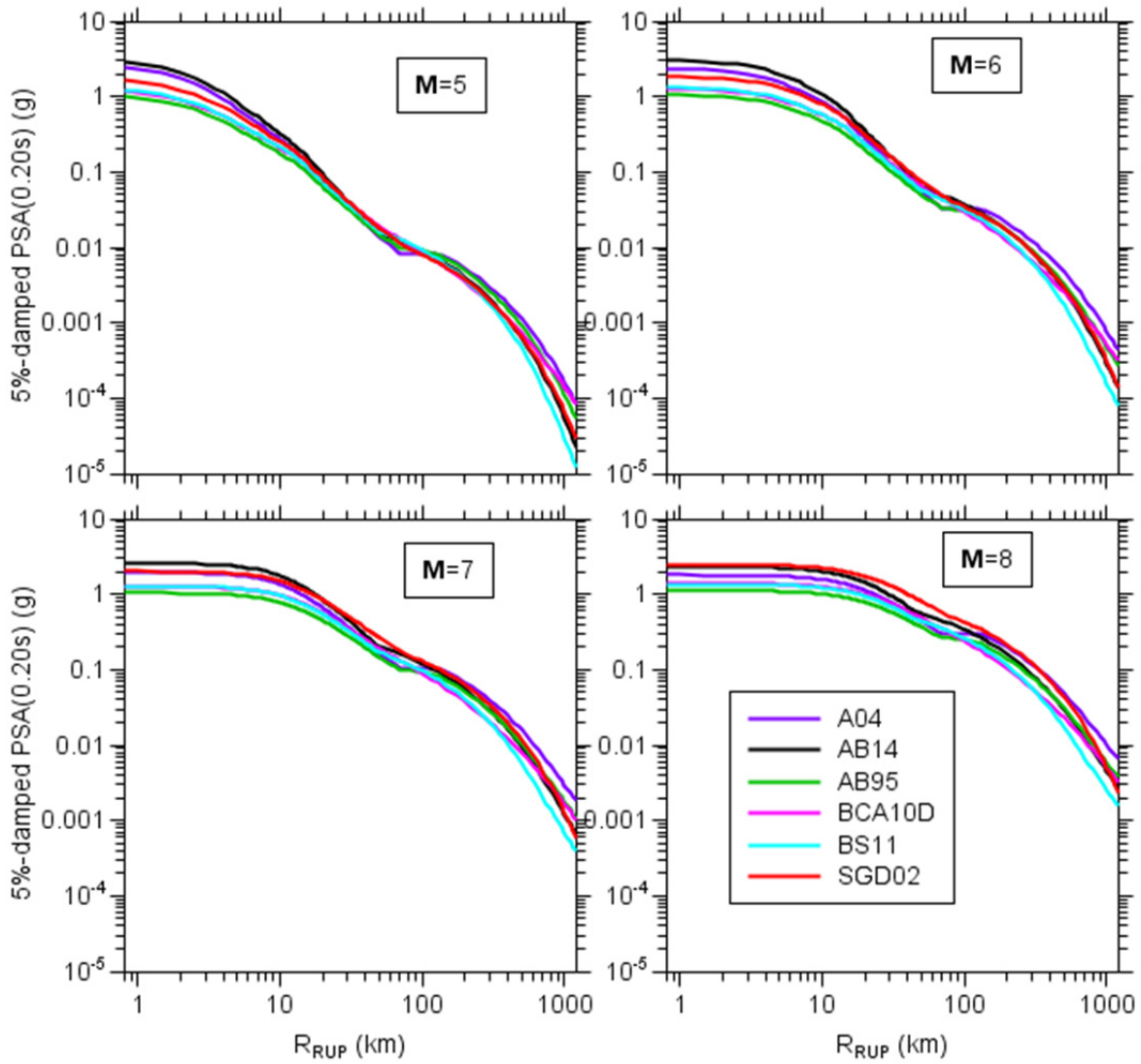
Figure 2.18   Simulated 5%-damped response spectra at a period of 0.01 sec for the Boatwright and Seekins [2011] (BS11) attenuation model as a function of distance to the rupture surface (R_{RUP}) for four magnitudes. Two magnitude-dependent functions for the finite-fault factor (FFF) were used to convert R_{RUP} to the distance R_{PS} used in the point-source simulations: Boore and Thompson [2015] solid lines and Yenier and Atkinson [2015a] dashed lines. The "scr" after BT15 and YA15 indicate that the FFFs were adjusted for SCRs, following BT15. The crustal amplifications used in the simulations were for sites with $V_{S30} = 3.0$ km/sec.

Figure 2.19 Simulated 5%-damped response spectra at a period of 0.1 sec for the Boatwright and Seekins [2011] (BS11) attenuation model as a function of distance to the rupture surface (R_{RUP}) for four magnitudes. Two magnitude-dependent functions for the finite-fault factor (FFF) were used to convert R_{RUP} to the distance R_{PS} used in the point-source simulations: Boore and Thompson [2015] solid lines and Yenier and Atkinson [2015a] dashed lines. The "scr" after BT15 and YA15 indicate that the FFFs were adjusted for stable continental regions (scr), following BT15. The crustal amplifications used in the simulations were for sites with $V_{S30} = 3.0$ km/sec .

Figure 2.20   Simulated 5%-damped response spectra at a period of 0.2 sec for the Boatwright and Seekins [2011] (BS11) attenuation model as a function of distance to the rupture surface (R_{RUP}) for four magnitudes. Two magnitude-dependent functions for the finite-fault factor (FFF) were used to convert R_{RUP} to the distance R_{PS} used in the point-source simulations: Boore and Thompson [2015] solid lines and Yenier and Atkinson [2015a] dashed lines. The "scr" after BT15 and YA15 indicate that the FFFs were adjusted for stable continental regions (scr), following BT15. The crustal amplifications used in the simulations were for sites with $V_{S30} = 3.0$ km/sec .
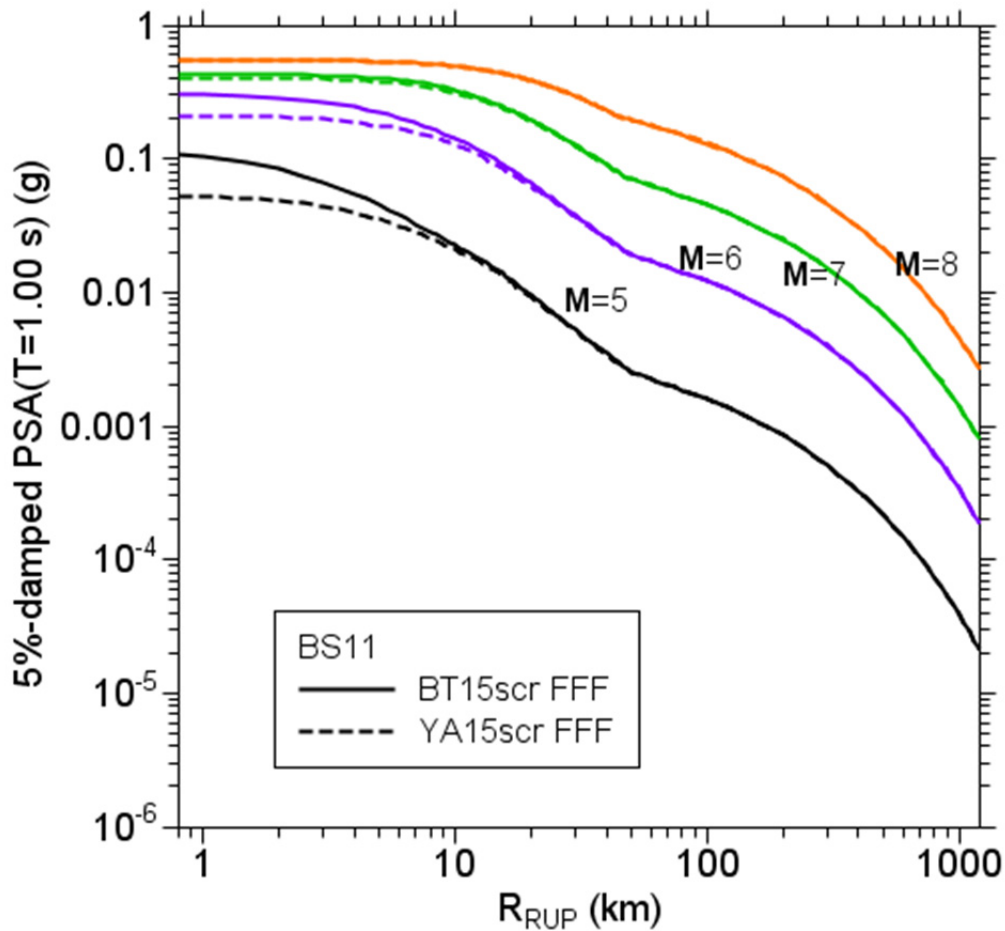
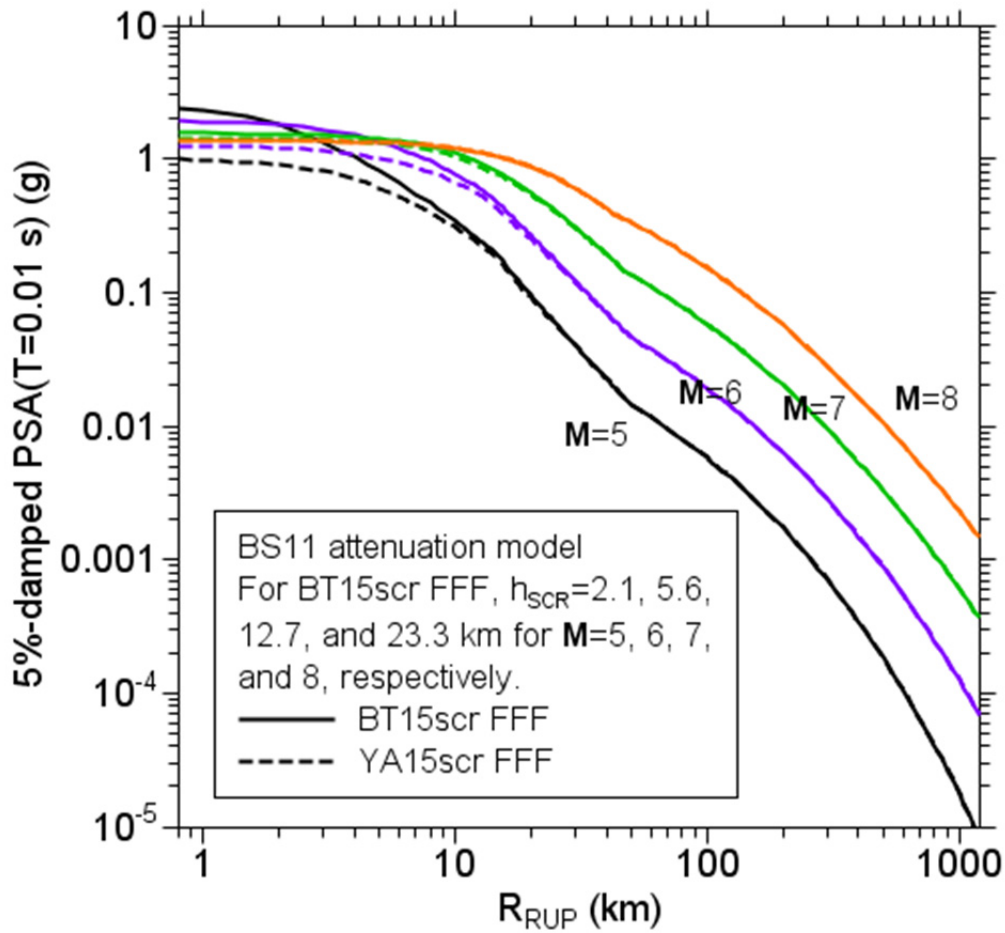**Figure 2.21** Simulated 5%-damped response spectra at a period of 1.0 sec for the Boatwright and Seekins [2011] (BS11) attenuation model as a function of distance to the rupture surface (R_{RUP}) for four magnitudes. Two magnitude-dependent functions for the finite-fault factor (FFF) were used to convert R_{RUP} to the distance R_{PS} used in the point-source simulations: Boore and Thompson [2015] solid lines and Yenier and Atkinson [2015a] dashed lines. The "scr" after BT15 and YA15 indicate that the FFF were adjusted for stable continental regions (scr), following BT15. The crustal amplifications used in the simulations were for sites with $V_{S30} = 3.0$ km/sec.
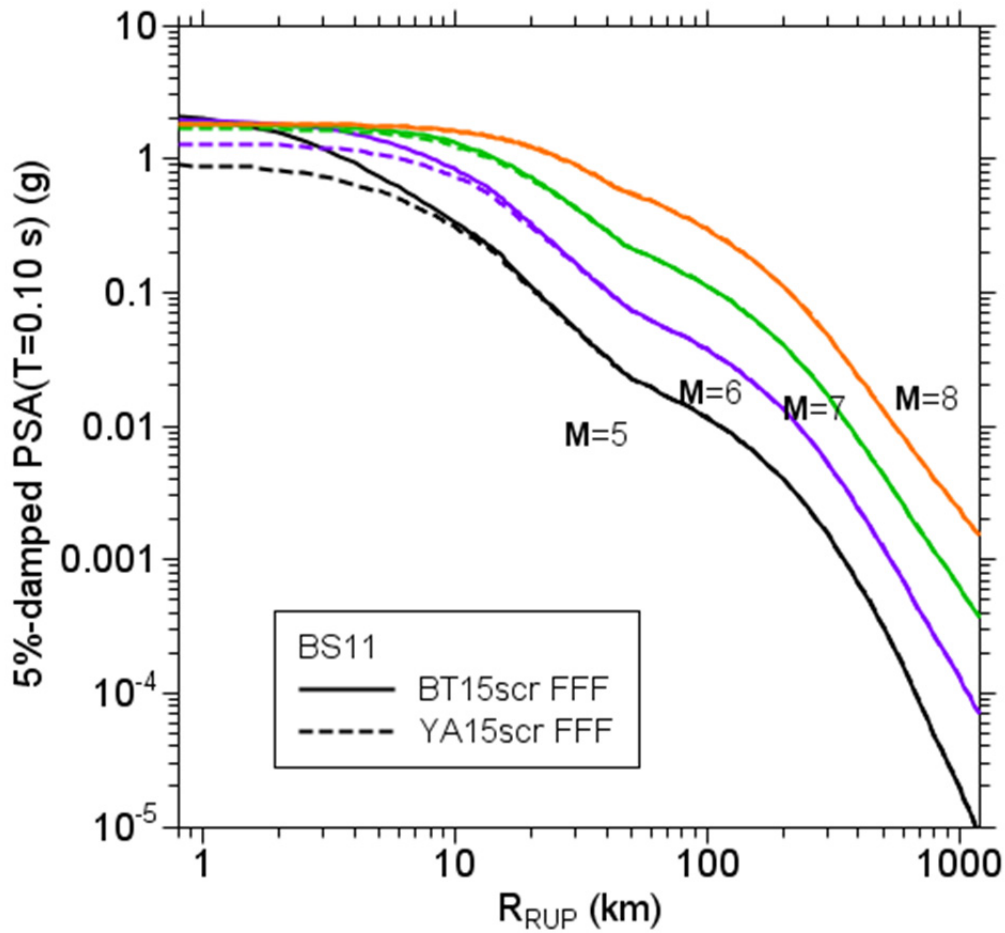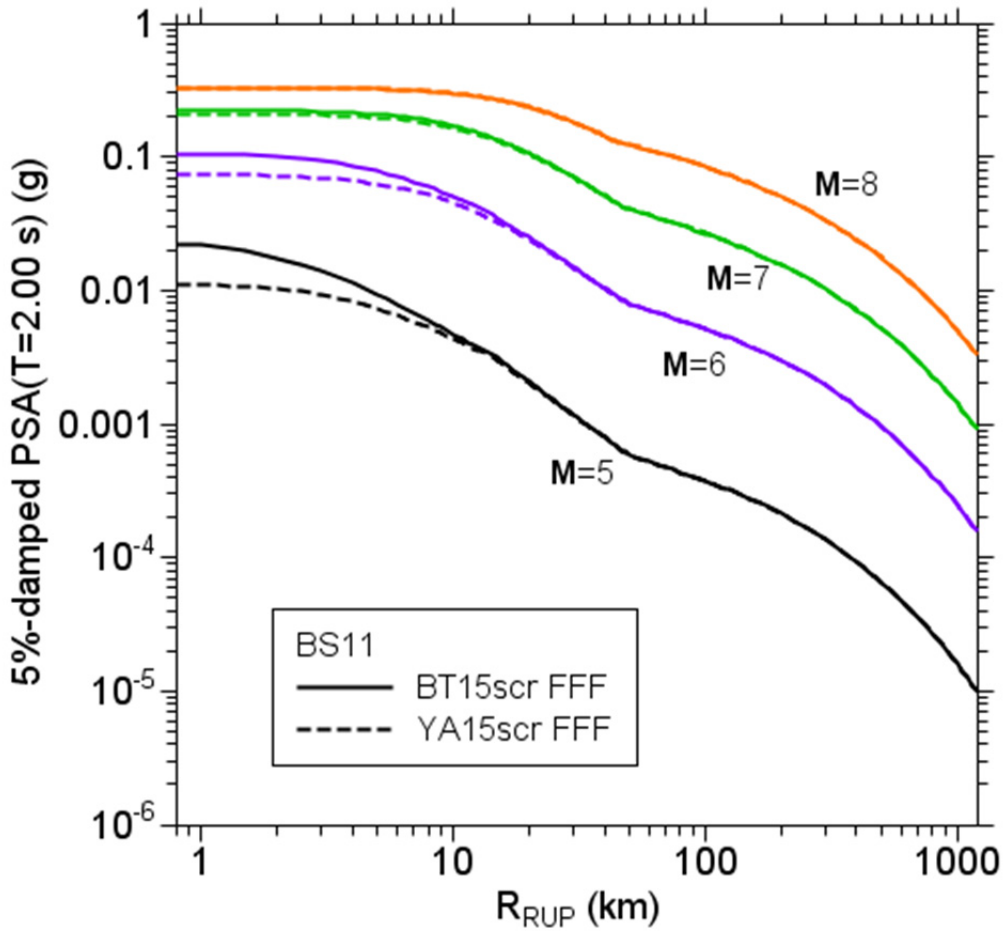
Figure 2.22 Simulated 5%-damped response spectra at a period of 2.0 sec for the Boatwright and Seekins [2011] (BS11) attenuation model as a function of distance to the rupture surface (R_{RUP}) for four magnitudes. Two magnitude-dependent functions for the finite-fault factor (FFF) were used to convert R_{RUP} to the distance R_{PS} used in the point-source simulations: Boore and Thompson [2015] solid lines) and Yenier and Atkinson [2015a] dashed lines). The "scr" after BT15 and YA15 indicate that the FFF were adjusted for stable continental regions (scr), following BT15. The crustal amplifications used in the simulations were for sites with $V_{S30} = 3.0$ km/sec .
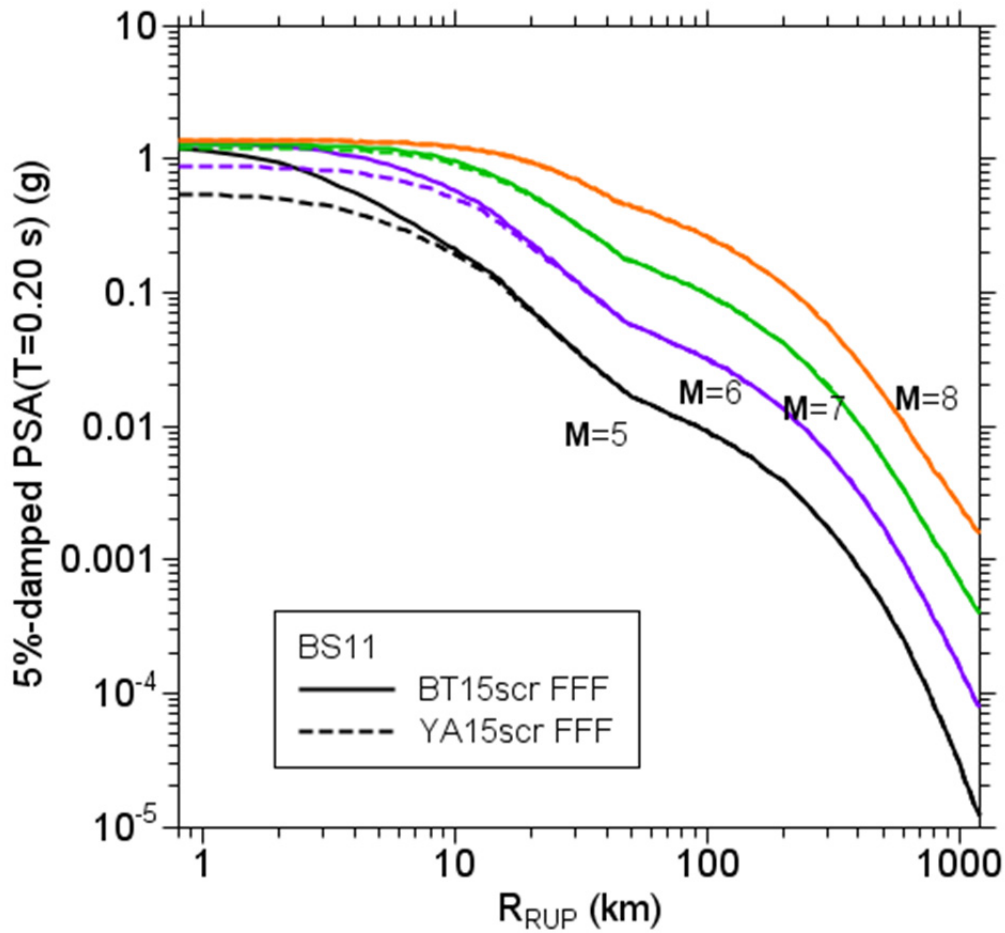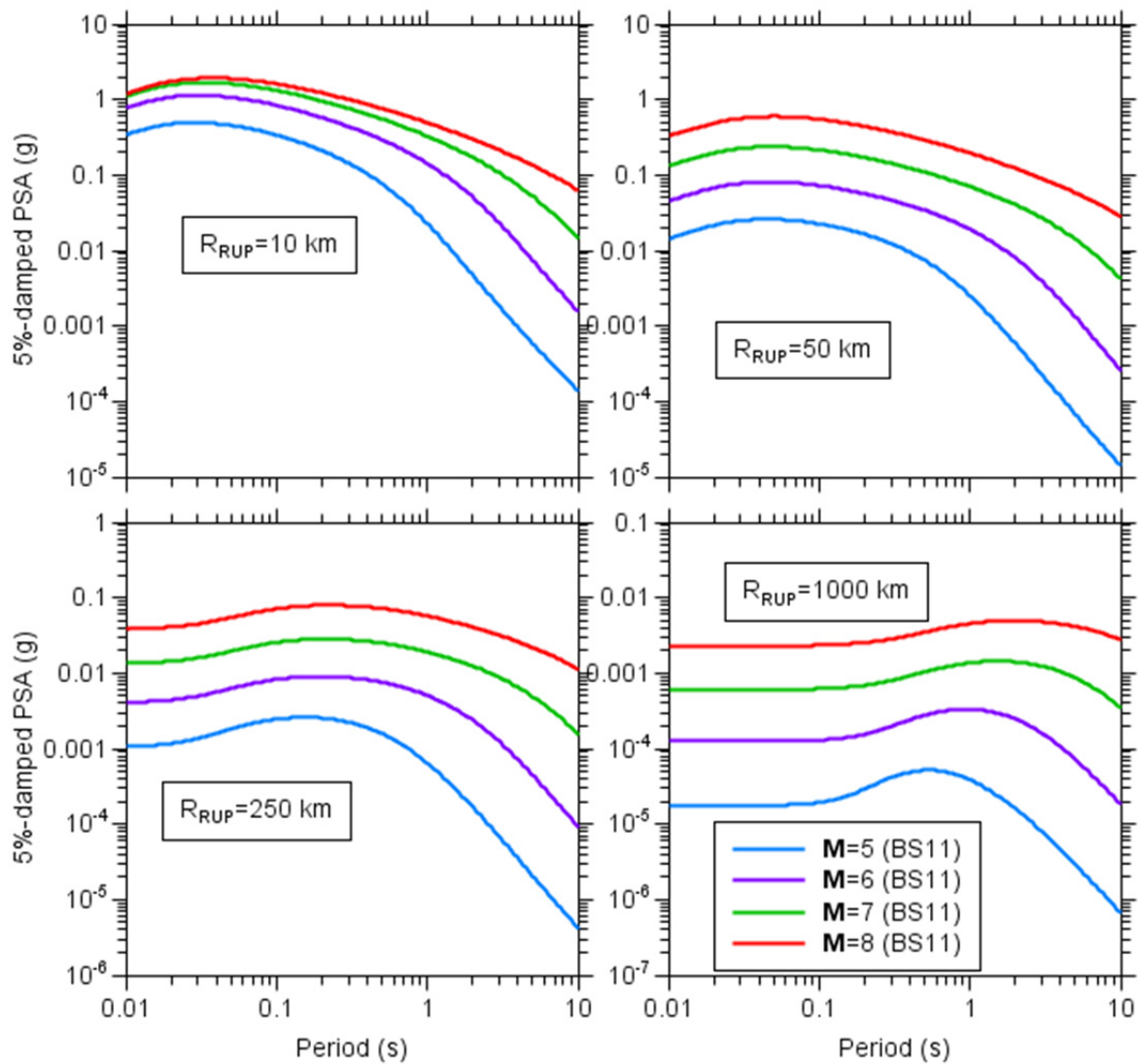
Figure 2.23   Simulated 5%-damped response spectra for the Boatwright and Seekins [2011] (BS11) attenuation model as a function of period for four magnitudes and four distances. The Boore and Thompson [2015] finite-fault factor for stable continental regions was used to convert R_{RUP} to the distance R_{PS} used in the point-source simulations. The crustal amplifications used in the simulations were for sites with $V_{S30} = 3.0$ km/sec .

2.5   SUMMARY AND DISCUSSION

In order to fulfill my commitment to the PEER NGA-East project, I have provided motions from point-source stochastic-method simulations for almost the whole stipulated range of $\mathbf{M}$, R, and T for the six specified attenuation models. Motions are not provided at all stipulated distances (R_{rup} from 0 to 1500 km) or magnitudes (up to 8.2), however, because the BT15 D_{RMS} coefficients are not defined for $R_{PS} < 2$ km and for $R_{PS} > 1262$ km and for $\mathbf{M} > 8.0$. The first distance condition means that motions are not provided for very short distances and small magnitudes, for which R_{PS} for the specified R_{RUP} is less than 2 km. The second distance condition means that no motions are provided for distances beyond 1262 km; because $R_{PS} \approx R_{RUP}$ at this distance, independent of magnitude, the exclusion applies for all magnitudes.

Even though I show that the models with $1/R^{1.3}$ geometrical spreading cannot fit longer period data no matter what stress parameter is used, I provide motions for those models anyway. Although I am not endorsing any one model, if I had to choose one, it would be the BS11 model. If I were allowed to choose three, they would be AB95, BCA10D, and BS11.

What Is Missing?

There are two obvious things missing from this report:

- a consideration of depth on the stress parameter
- a discussion of the uncertainty in the motions

There are some studies that find a depth dependence to the stress parameter, not only for potentially-induced earthquakes, but also for regular tectonic earthquakes (e.g., J. Boatwright, presentation given at a NGA-East workshop). I have not attempted to include such a dependence in this study, although it would be easy to do so. The second limitation—no discussion of uncertainty—would require more work, such as doing many simulations using distributions of the model parameters. These distributions would include the "static" parameters such as average radiation pattern, as well as "dynamic" parameters such as the stress parameter, whose distribution could be guided by *sdevfctr* in Tables 2.5–2.9.

2.6   ACKNOWLEDGMENTS

2.7 LIST OF ELECTRONIC APPENDICES FOR CHAPTER 2

2A   Sample Input file for SMSIM (PDF document)

2B   Model Output for A04 attenuation (Excel workbook)

2C   Model Output for AB14 attenuation (Excel workbook)

2D   Model Output for AB95 attenuation (Excel workbook)

2E   Model Output for BCA10D attenuation (Excel workbook)

2F   Model Output for BS11 attenuation (Excel workbook)

2G   Model Output for SGD02attenuation (Excel workbook)

12 REFERENCES

Abrahamson N.A., Silva W.J. (1997). Empirical response spectral attenuation relations for shallow crustal earthquakes, *Seismol. Res. Lett.,* 68(1): 94−127.

Abrahamson N.A., Silva W.J. (2001). Empirical attenuation relations for central and eastern U.S. hard and soft rock and deep soil site conditions, *Seism. Res. Lett.* **72**, 282.

Abrahamson N.A., Silva W.J, Kamai R. (2014). Summary of the ASK14 ground-motion relation for active crustal regions, *Earth. Spectra,* 30(3): 1025−1055,

Abrahamson N.A., Youngs R.R. (1992). A stable algorithm for regression analysis using the random effects model, *Bull. Seismol. Soc. Am.,* 82: 505−510.

Al Atil L. (2014). *Personal Communication.*

Al Atik L., Abrahamson N.A., Bommer J.J., Scherbaum F., Cotton F., Kuehn N. (2010). The variability of ground-motion prediction models and its components, *Seismol. Res. Lett.,* 81: 794−801.

Al Atik L., Kottke A., Abrahamson N.A., Hollenback J. (2014). Kappa (k) scaling of ground-motion prediction equations using an inverse random vibration theory approach, *Bull. Seismol. Soc. Am.,* 104: 336−346.

Al Atik L., Youngs R.R. (2014). Epistemic uncertainty for NGA-West2 models, *Earthq. Spectra,* 30(3): 1301−1318.

Al Noman M.N. [2013]. *Ground Motion Modeling for Eastern North America: An Empirical Approach with the NGA-East Database,* M.S. thesis, University of Memphis, 54 pgs.

Allen T., Cummins P., Dhu T., Schneider J. (2007). Attenuation of ground-motion spectral amplitudes in southeastern Australia, *Bull. Seismol. Soc. Am.,* 97: 1279−1292.

Ancheta T., Darragh R.B., Stewart J.P., Seyhan E., Silva W.J., Chiou B.-S.J., Wooddell K., Graves R.W., Kottke A.R., Boore D.M., Kishida T., Donahue J. (2014). PEER NGAWest2 database, *Earthq. Spectra,* 30: 989−1006.

Andrews D.J. (1980). A stochastic fault model: 1. Static case, *J. Geophys. Res.,* 85: 3867−3877.

Anderson J.G., Hough S.E. (1984). A model for the shape of the Fourier amplitude spectrum of acceleration at high frequencies, *Bull. Seismol. Soc. Am.,* 74(5): 1969−1993.

Assatourians K., Atkinson G.M. (2010). Database of processed time series and response spectra data for Canada: An example application to study of 2005 MN5.4 Riviere du Loup, Quebec, earthquake, *Seismol. Res. Lett.,* 81, 1013−1031.

Atkinson G.M. (2001). An alternative to stochastic ground-motion relations for use in seismic hazard analysis in eastern North America, *Seismol. Res. Lett.,* 72: 299−306.

Atkinson G.M. (2004). Empirical attenuation of ground-motion spectral amplitudes in southeastern Canada and the northeastern United States, *Bull. Seismol. Soc. Am.,* 94: 1079−1095.

Atkinson G.M. (2005). Ground motions for earthquakes in southwestern British Columbia and northwestern Washington: crustal, in-slab, and offshore events, *Bull. Seismol. Soc. Am.,* 95: 1027−1044.

Atkinson G M. (2008). Ground motion prediction equations for eastern North America from a referenced empirical approach: Implications for epistemic uncertainty, *Bull. Seismol. Soc. Am.,* 98: 1304−1318.

Atkinson G.M. (2010). Ground-motion prediction equations for Hawaii from a referenced empirical approach, *Bull. Seismol. Soc. Am.,* 101: 1304–1318.

Atkinson G.M. (2012a). Evaluation of attenuation models for the northeastern United States/southeastern Canada, *Seismol. Res. Lett.* 83, 166–178.

Atkinson G.M. (2012b). White paper on proposed ground-motion prediction equations (GMPEs) for 2015 national seismic hazard maps, *http://www.seismotoolbox.ca/GMPEtables2012/r12_GMPEs9b.pdf* (last accessed in January 2015).

Atkinson G.M. (2013). Empirical evaluation of aleatory and epistemic uncertainty in eastern ground motions, *Seismol. Res. Lett.*, 84: 130–138.

Atkinson G.M., Assatourians K. (2010). Attenuation and source characteristics of the 23 June 2010 **M** 5.0 Val-des-Bois, Quebec, earthquake, *Seismol. Res. Lett.*, 81: 849–860.

Atkinson G.M., Assatourians, K. (2015). Implementation and validation of EXSIM (a stochastic finite-fault ground-motion simulation algorithm) on the SCEC broadband platform, *Seismol. Res. Lett.*, 86(1): 48–60.

Atkinson G.M., Babaie Mahani A. (2013). Estimation of moment magnitude from ground motions at regional distances, *Bull. Seismol. Soc. Am.*, 103: 107–116.

Atkinson G.M., Bommer J.J., Abrahamson N.A. (2014). Alternative approaches to modeling epistemic uncertainty in ground motions in probabilistic seismic hazard analysis, *Seismol. Res. Lett.*, 85: 1141–1144.

Atkinson G.M., Boore D.M. (1995). Ground motion relations for eastern North America, *Bull. Seismol. Soc. Am.*, 85: 17–30.

Atkinson G.M., Boore D.M. (1997). Some comparisons between recent ground-motion relations, *Seismol. Res. Lett.,* 68(1): 24–40.

Atkinson G.M., Boore D.M. (2006). Earthquake ground-motion prediction equations for eastern North America, *Bull. Seismol. Soc. Am.*, 96: 2181–2205.

Atkinson G.M., Boore D.M. (2011). Modification to existing ground-motion prediction equations in light of new data, *Bull. Seismol. Soc. Am.*, 101(3): 1121–1135.

Atkinson G.M. Boore D.M. (2014). The attenuation of Fourier amplitudes for rock sites in eastern North America, *Bull. Seismol. Soc. Am.*, 104: 513–528.

Atkinson G.M., Boore D.M., Assatourians K., Campbell K.W., Motazedian D. (2009). A guide to differences between stochastic point-source and stochastic finite-fault simulations, *Bull. Seismol. Soc. Am.*, 99: 3192–3201.

Atkinson G.M., Greig D., Yenier E. (2014). Estimation of moment magnitude (M) for small events (M<4) on local networks, *Seismol. Res. Lett.*, 85: 1116–1124.

Atkinson G.M., Mereu R. (1992). The shape of ground motion attenuation curves in southeastern Canada, *Bull. Seismol. Soc. Am.*, 82: 2014–2031.

Atkinson G.M., Morrison M. (2009). Regional variability in ground motion amplitudes along the west coast of North America, *Bull. Seismol. Soc. Am.*, 99: 2393–2409.

Atkinson G.M., Motazedian D. (2013). Ground-motion amplitudes for earthquakes in Puerto Rico, *Bull. Seismol. Soc. Am.*, 103: 1846–1859.

Atkinson G.M., Silva W.J. (1997). An empirical study of earthquake source spectra for California earthquakes, *Bull. Seismol. Soc. Am.*, 87: 97–113.

Atkinson G.M., Silva W.J. (2000). Stochastic modeling of California ground motions, *Bull. Seismol. Soc. Am.*, 90: 255–274.

Atkinson G.M., Wald D.J. (2007). "Did you feel it?" intensity data: a surprisingly good measure of earthquake ground motion, *Seismol. Res. Lett.*, 78: 362–368.

Babaie Mahani A., Atkinson G.M. (2012). Evaluation of functional forms for the attenuation of small-to-moderate-earthquake response spectral amplitudes in North America, *Bull. Seismol. Soc. Am.* 102: 2714–2726.

Babaie Mahani A., Atkinson G.M. (2013). Regional differences in ground-motion amplitudes of small-to-moderate earthquakes across North America, *Bull. Seismol. Soc. Am*., 103(5): 2604–2620.

Bakun W.H. Hopper M.G. (2004). Magnitudes and locations of the 1811–1812 New Madrid, Missouri, and the 1886 Charleston, South Carolina, Earthquakes, *Bull. Seismol. Soc. Am.*, 94: 64–75.

Baltay A.S., Hanks T.C. (2014). Understanding the magnitude dependence of PGA and PGV in NGA-West2 Data, *Bull. Seismol. Soc. Am.*, 104: 2851–2865.

Bent A.L. (1992). A re-examination of the 1925 Charlevoix, Quebec, earthquake, *Bull. Seismol. Soc. Am.*, 82: 2097–2113.

Bent, A.L. (1995). A complex double-couple source mechanism for the Ms 7.2 1929 Grand Banks earthquake, *Bull. Seismol. Soc. Am.*, 85: 1003–1020.

Beresnev I.A., Atkinson G.M. (1999). Generic finite-fault model for ground motion prediction in eastern North America, *Bull. Seismol. Soc. Am*., 89: 608–625.

Beresnev I.A., Atkinson G.M. (2002). Source parameters of earthquakes in eastern and western North America based on finite–fault modeling, *Bull. Seismol. Soc. Am*., 92: 695–710.

Boatwright J., Seekins L. (2011). Regional spectral analysis of three moderate earthquakes in northeastern North America, *Bull. Seismol. Soc. Am.*, 101: 1769–1782.

Bodin, P., Malagnini L., Akinci A. (2004). Ground-motion scaling in the Kachchh Basin, India, deduced from aftershocks of the 2001 Mw 7.6 Bhuj earthquake, *Bull. Seismol. Soc. Am.*, 94: 1658–1669.

Bommer, J., Stafford P., Alarcon J., Akkar S. (2007). The influence of magnitude range on empirical ground-motion prediction, *Bull. Seismol. Soc. Am*., 97: 2152–2170.

Boore D.M. (1983). Stochastic simulation of high-frequency ground motions based on seismological models of the radiated spectra, *Bull. Seismol. Soc. Am*., 73: 1865–1894.

Boore D.M. (2003). Prediction of ground motion using the stochastic method, *Pure Appl. Geophys.* 160: 635–676.

Boore D.M. (2005). SMSIM—Fortran programs for simulating ground motions from earthquakes: Version 2.3—A revision of OFR 96-80-A, U.S. Geological Survey open-file report, *U. S. Geological Survey Open-File Report 00-509*, revised 15 August 2005, 55 pgs.

Boore D.M. (2009). Comparing stochastic point-source and finite-source ground-motion simulations: SMSIM and EXSIM, *Bull. Seismol. Soc. Am.,* 99; 3202–3216.

Boore D.M. (2010). Orientation-independent, non geometric-mean measures of seismic intensity from two horizontal components of motion, *Bull. Seismol. Soc. Am.,* 100: 1830–1835.

Boore D.M. (2012). Updated determination of stress parameters for nine well-recorded earthquakes in Eastern North America, *Seismol. Res. Lett.,* 83: 190–199.

Boore D.M. (2013). The uses and limitations of the square-root impedance method for computing site amplification, *Bull. Seismol. Soc. Am.*, 103: 2356–2368.

Boore D.M. (2015). Adjusting PSA amplitudes to $V_{S30} = 3.0$ km/sec , PEER Report, *in preparation*.

Boore D.M., Atkinson G.M. (1987). Stochastic prediction of ground motion and spectral response parameters at hard-rock sites in eastern North America, *Bull. Seismol. Soc. Am.*, 77(2): 440-467.

Boore D.M., Boatwright J. (1984). Average body-wave radiation coefficients, *Bull. Seismol. Soc. Am.*, 74: 1615–1621.

Boore D.M., Campbell K.W., Atkinson G.M. (2010). Determination of stress parameters for eight well-recorded earthquakes in eastern North America, *Bull. Seismol. Soc. Am.,* 100: 1632–1645.

Boore D.M., Di Alessandro C., Abrahamson N.A. (2014a). A generalization of the double-corner-frequency source spectral model and its use in the SCEC BBP validation exercise, *Bull. Seismol. Soc. Am.*, 104: 2387–2398.

Boore D.M., Joyner W.B. (1997). Site amplifications for generic rock sites, *Bull. Seismol. Soc. Am.*, 87: 327–341.

Boore D.M., Stewart J.P., Seyhan E., Atkinson G.M. (2014b). NGA-West2 equations for predicting response spectral accelerations for shallow crustal earthquakes, *Earthq. Spectra*, 30: 1057−1085.

Boore D.M., Thompson E.M. (2014). Path durations for use in the stochastic-method simulation of ground motions, *Bull. Seismol. Soc. Am.*, 104: 2541–2552. DOI: 10.1785/0120140058

Boore D.M., Thompson E.M. (2015). Revisions to some parameters used in stochastic-method simulations of ground motion, *Bull. Seismol. Soc. Am.,* Vol. 105 (in press).

Boore, D.M., Watson-Lamprey J., Abrahamson N.A. (2006). Orientation-independent measures of ground motion, *Bull. Seismol. Soc. Am.*, 96: 1502–1511.

Bora S.S., Scherbaum F., Kuehn N., Stafford P. (2014) Fourier spectral- and durations models for the generation of response spectra adjustable to different source-, propagation-, and site conditions, *Bull Earthq. Eng.*, 12: 467–493.

Bozorgnia Y., Abrahamson N.A., Al Atik L., Ancheta T.D., Atkinson G.M., Baker J., Baltay A., Boore D.M, Campbell K.W., Chiou B.-S.J., Darragh R.B., Day S., Donahue J., Graves R.W., Gregor N., Hanks T., Idriss I.M., Kamai R., Kishida T., Kottke A., Mahin S.A., Rezaeian S., Rowshandel B., Seyhan E., Shahi S., Shantz T., Silva W.J., Spudich P., Stewart J.P., Watson-Lamprey J., Wooddell K.E., Youngs R.R. (2014). NGA-West2 research project, *Earthq. Spectra*, 30(3): 973–987.

Brune J.N. (1970). Tectonic stress and the spectra of seismic shear waves from earthquakes, *J. Geophys. Res.*, 75: 4997–5009.

Brune, J. (1971). Correction, *J. Geophys. Res.*, 76: 5002.

BSSC (2009). NEHRP Recommended Seismic Provisions for New Buildings and Other Structures (FEMA P-75), 2009 ed., Building Seismic Safety Council, Washington, D.C.

Burger R.W., Somerville P.G., Barker J.S., Herrmann R.B., Helmberger D.V. (1987). The effect of crustal structure on strong ground motion attenuation relations in eastern North America, *Bull. Seismol. Soc. Am.*, 77: 420–439.

Campbell, K. W. (1981). A ground motion model for the central United States based on near source acceleration data, in Proceedings of the Conference on Earthquakes and Earthquake Engineering—the Eastern United States, Ann Arbor Science Publishers, Ann Arbor, Michigan, Vol. 1, 213–232.

Campbell K.W. (2002). Development of semi-empirical attenuation relationships for the CEUS, Report to U.S. Geological Survey, *NEHRP Award No.01HQGR0011*.

Campbell K.W. (2003). Prediction of strong ground motion using the hybrid empirical method and its use in the development of ground-motion (attenuation) relations in eastern North America, *Bull. Seismol. Soc. Am.*, 93: 1012–1033.

Campbell K.W. (2007). Validation and update of hybrid empirical ground motion (attenuation) relations for the CEUS, report to the U.S. Geological Survey, *National Earthquake Hazards Reduction External Research Program*, *Award No. 05HQGR0032*.

Campbell K.W. (2008). Hybrid empirical ground motion model for PGA and 5% damped linear elastic response spectra from shallow crustal earthquakes in stable continental regions: Example for eastern North America, *Proceedings, 14th World Conference on Earthquake Engineering*, Paper No. S03-001, Beijing, China.

Campbell K.W. (2009). Estimates of shear-wave Q and κ_0 for unconsolidated and semiconsolidated sediments in eastern North America, *Bull. Seismol. Soc. Am.*, 99: 2365–2392.

Campbell K.W. (2011). Ground motion simulation using the hybrid empirical method: Issues and insights, in *Earthquake Data in Engineering Seismology: Predictive Models, Data Management and Networks*, S. Akkar, P. Gulkan, T. van Eck (eds.), Geotechnical, Geological and Earthquake Engineering Series, Springer, London, 14: 81–95.

Campbell K.W. (2014). An evaluation of eastern North America ground-motion models developed using the hybrid empirical method, *Bull. Seismol. Soc. Am.*, 104: 347–359.

Campbell K.W., Bozorgnia Y. (2008). NGA ground motion model for the geometric mean horizontal component of PGA, PGV, PGD and 5% damped linear-elastic response spectra for periods ranging from 0.01 to 10.0 s, *Earthq. Spectra*, 24: 139–171.

Campbell K.W., Bozorgnia Y. (2014). NGA-West2 ground motion model for the average horizontal components of PGA, PGV, and 5% damped linear acceleration response spectra, *Earthq. Spectra,* 30(3): 1087–1115.

Campbell K.W., Hashash Y.M.A., Kim B., Kottke A.R., Rathje E.M., Silva W.J., Stewart J.P. (2014). Reference-rock site conditions for Central and Eastern North America: Part II – Attenuation definition, *PEER Report 2014-12*, Pacific Earthquake Engineering Research Center, University of California, Berkeley, CA, 80 pgs.

Chapman M.C. (2013). On the rupture process of the 23 August 2011 Virginia earthquake, *Bull. Seismol. Soc. Am.*, 103: 613–628.

Chapman M.C., Godbee R.W. (2012). Modeling geometrical spreading and the relative amplitudes of vertical and horizontal high-frequency ground motions in eastern North America, *Bull. Seismol. Soc. Am.*, 102: 1957–1975.

Chapman M.C, Pezeshk S., Hosseini M., Conn A. (2014). Regional study of Fourier amplitude drop of *Lg*-wave acceleration in central United States, *Proceedings, Seismological Society of America Annual Meeting*, Anchorage, AK.

Chiou B.-S.J., Youngs R.R. (2014). Update of the Chiou and Youngs NGA model for the average horizontal component of peak ground motion and response spectra, *Earthq. Spectra,* 30(3): 1117–1153.

Chun K., West G.F., Kokoski R.J., Samson C. (1987) A novel technique for measuring *Lg* attenuation results from Eastern Canada Between 1 to 10 Hz, *Bull. Seismol. Soc. Am.,* 77(2): 398–419.

Cramer C.H., Al Noman M.N., DeShon H.R. (2014). Improving regional ground motion attenuation boundaries and models using EarthScope USArray data for use in the National Seismic Hazards Mapping Project, *Final Technical Report to the USGS under grant G12AP20018*, 19 pgs.

Cramer C.H., Boyd O.S. (2014). Why the New Madrid earthquakes are M7-8 and the Charleston earthquake is ~M7, *Bull. Seismol.. Soc. Am.*, 104: 2884–2903.

Cramer C.H., Kumar A. (2003). 2001 Bhuj, India earthquake engineering seismoscope recordings and eastern North America ground-motion attenuation relations, *Bull. Seismol. Soc. Am.,* **93**, 1390–1394.

Cramer C.H., Kutliroff J.R., Dangkua D.T. (2011). *Next Generation Attenuation East Initial Flat Files for Eastern North America*, *Report to PEER accompanying NGA-East flat files and time series under subagreement 7140,*

Cramer, C.H., Kutliroff, J.R., Dangkua, D.T., and Al Noman, M.N. (2013). *Completing the NGA-East CENA/SCR Ground Motion Database*, Report prepared for the Pacific Earthquake Engineering Research Center by the Center for Earthquake Research and Information, University of Memphis under Subagreement 7140, April 5, 2013, 18 pgs.,
https://umdrive.memphis.edu/ccramer/public/NGAeast/ Documentation/NGAEastDbPEERFinalReport.docx

Der Kiureghian A. (1980). Structural response to stationary excitation, *J. Eng. Mech. Div.,* EM6: 1195–1213.

Douglas J. (2003). Earthquake ground motion estimation using strong-motion records: A review of equations for the estimation of peak ground acceleration and response spectral ordinates, *Earth-Science Reviews*, 61(1–2): 43–104.

Douglas J. (2004). An investigation of analysis of variance as a tool for exploring regional differences in strong ground motions, *J. Seismol*., 8: 484–496.

Douglas J. (2011). Ground motion prediction equations 1964–2010, *PEER Report 2011/102,* Pacific Earthquake Engineering Research Center, University of California, Berkeley, CA.

Douglas J., Bungum H., Scherbaum F. (2006). Ground-motion prediction equations for southern Spain and southern Norway obtained using the composite model perspective. *J. Earthq. Eng.,*10: 33–72.

Dreger D.S., Beroza G.C., Day S.M., Goulet C.A., Jordan T.H., Spudich PA., Stewart J.P. (2015). Validation of the SCEC broadband platform v14.3 simulation methods using pseudospectral acceleration data, *Seismol. Res Lett*. 86: 39–47.

Dreiling J., Isken M.P., Mooney W.D., Chapman M.C., Godbee R.W. (2014). *NGA-East* regionalization report: comparison of four crustal regions within central and eastern north america using waveform modeling and 5%-

damped pseudo-spectral acceleration response, *PEER Report No. 2014/15*, Pacific Earthquake Engineering Research Center, University of California, Berkeley, CA.

Erickson D., McNamara D.E., Benz H.M. (2004). Frequency-dependent Lg *Q* within the continental United States. *Bull. Seismol. Soc. Am.*, 94: 1630−1643.

EPRI (1993). Guidelines for determining design basis ground motions, *EPRI TR-102293*, Vol 1−5, Electric Power Research Institute, Palo Alto, CA.

EPRI (2004). CEUS ground motion project final report. *Technical Report 100968,*. Electric Power Research Institute, Dominion Energy, Glen Allen, VA, Entergy Nuclear, Jackson, MS, and Exelon Generation Company, Kennett Square, PA. Palo Alto, CA

EPRI (2006). Program on Technology Innovation: Truncation of the Lognormal Distribution and Value of the Standard Deviation for Ground Motion Models in the Central and Eastern United States, EPRI Report 1013105, Technical Update, February, Palo Alto, Calif.

EPRI (2013). EPRI 2004-2006 Ground-Motion Model (GMM) Review Project 3002000717, Final Report. June 2013, Electric Power Research Institute, Palo Alto, CA.

EPRI/DOE/NRC (2012). Technical Report: Central and Eastern United States Seismic Source Characterization for Nuclear Facilities, NUREG-2115.

Fatehi A., Herrmann R.B. (2008). High-frequency ground-motion scaling in the Pacific Northwest and in northern and central California, *Bull. Seismol. Soc. Am.*, 98: 709–721.

Frankel A. (1995). Simulating strong motions of large earthquakes using recordings of small earthquakes: the Loma Prieta mainshock as a test case, *Bull. Seismol. Soc. Am.,* 85: 1144−1160.

Frankel A. (2009). A constant stress-drop model for producing broadband synthetic seismograms—Comparison with the Next Generation Attenuation Relations, *Bull. Seismol. Soc. Am.*, 99: 664−681.

Frankel A. (2013). Rupture history of the 2011 M9 Tohoku Japan earthquake determined from strong-motion and high-rate GPS recordings, sub-events radiating energy in different frequency bands, *Bull. Seismol. Soc. Am.*, 103: 1290−1306.

Frankel A. (2015). Decay of S-wave amplitudes with distance for earthquakes in the Charlevoix, Quebec area: effects of radiation pattern and directivity, *Bull. Seismol. Soc. Am.*, DOI.101785/0120140249.

Frankel A., Mueller, C. Barnhard T., Perkins D., Leyendecker E.V., Dickman N., Hanson S., Hopper M. (1996). National seismic hazard maps—Documentation June 1996, *U.S. Geological Survey Open File Report 96-532,* Menlo Park, CA, 110 pgs.

Ghodrati G., Shahjouei A., Saadat S., Ajallooeian M. (2011). Implementation of genetic algorithm, MLFF neural network, principal component analysis and wavelet packet transform in generation of compatible seismic ground acceleration time histories, *J. Earthq. Eng.*, 15(1): 50–76.

Goldstein P., Dodge D., Firpo M., Minner L. (2003). SAC2000: Signal processing and analysis tools for seismologists and engineers, Invited contribution to *The IASPEI International Handbook of Earthquake and Engineering Seismology*, Edited by W.H.K. Lee, H. Kanamori, P.C. Jennings, and C. Kisslinger (eds.), Academic Press, London.

Goulet C.A., Boore D.M. (2014). *Personal Communication*.

Goulet C.A., Abrahamson N.A., Somerville P.G., Wooddell K.E. (2015). The SCEC broadband platform validation exercise: Methodology for code validation in the context of seismic hazard analyses, *Seismol. Res. Lett.*, 86(1): 17–26.

Goulet C.A., Kishida T. Ancheta T D., Cramer C.H., Darragh R.B., Silva W.J., Hashash Y.M.A., Harmon J., Stewart J.P., Wooddell K.E., Youngs R.R. (2014). PEER NGA-East database, *PEER Report 2014/17,* Pacific Earthquake Engineering Research Center, University of California, Berkeley, CA.

Graizer V. (2014a). Updated Graizer-Kalkan ground-motion prediction equations for Western United States, *Proceedings, 10th National Conference on Earthquake Engineering*, Earthquake Engineering Research Institute, Anchorage, AK.

Graizer V. (2014b). Preliminary ground motion prediction equations for the Central and Eastern United States. Abstract, *American Geophysical Union Annual Meeting*, San Francisco, CA.

Graizer V. Kalkan E. (2007). Ground-motion attenuation model for peak horizontal acceleration from shallow crustal earthquakes, *Earthq. Spectra*, 23(3): 585−613.

Graizer V. Kalkan E. (2009). Prediction of response spectral acceleration ordinates based on PGA attenuation, *Earthq. Spectra*, 25(1): 39−69.

Graizer V. Kalkan E. (2011). Modular filter-based approach to ground-motion attenuation modeling, *Seismol. Res. Lett.*, 82(1): 21−31.

Graizer V. Kalkan E. (2015). Update of the Graizer-Kalkan ground-motion prediction equations for shallow crustal continental earthquakes**, *U.S. Geological Survey Open-File Report 2015-1009*, http://dx.doi.org/10.3133/ofr20151009.

Graves R.W., Pitarka A. (2004). Broadband time history simulation using a hybrid approach, *Proceedings, 13th World Conference on Earthquake Engineering*, Paper No., 1098. Vancouver, B.C., Canada.

Graves R.W., Pitarka A. (2010). Broadband ground-motion simulation using a hybrid approach, *Bull. Seismol. Soc. Am.*, 100: 1197−1210.

Graves R.W., Pitarka A. (2015). Refinements to the Graves and Pitarka (2010) broadband ground motion simulation method, *Seismol. Res. Lett.*, 86(1) 75−80.

Gregor N., Abrahamson N.A., Atkinson G.M., Boore D.M., Bozorgnia Y., Campbell K.W, Chiou B.-S.J., Idriss I.M., Kamai R., Seyhan E., Silva W.J., Stewart J.P., Youngs R.R. (2014). Comparison of NGA-West 2 GMPEs, *Earthq. Spectra*, 30: 1179−1197.

Hanks T.C. (1982). f_{max}, *Bull. Seismol. Soc. Am.,* 72: 1867−1879.

Hanks T.C., Bakun W.H. (2002). A bilinear source-scaling model for M–log A observations of continental earthquakes, *Bull. Seismol. Soc. Am.*, 92: 1841−1846.

Hanks T.C., Kanamori H. (1979). A moment magnitude scale, *J. Geophys. Res.*, 84: 2348−2350.

Hanks T.C., McGuire R.K. (1981). The character of high–frequency strong ground motion, *Bull. Seismol. Soc. Am.,* 71: 2071−2095.

Hartzell S.W., Langer C., Mendoza C. (1994). Rupture histories of Eastern North American earthquakes, *Bull. Seismol. Soc. Am.,* 84(6): 1703−1724.

Hartzell S.H., Frankel A., Liu P., Zeng Y., Rahman S. (2011). Model and parametric uncertainty in source-based kinematic models of earthquake ground motion, *Bull. Seismol. Soc. Am.*, 101: 2431−2452.

Hartzell S.H., Guatteri M., Mariagiovanna G., Mai P.M., Liu P.C., Fisk M. (2005). Calculation of broadband time histories of ground motion, Part II: Kinematic and dynamic modeling using theoretical Green's functions and comparison with the 1994 Northridge earthquake, *Bull. Seismol. Soc. Am.*, 95: 614–645.

Hartzell S.H., Harmsen S., Frankel A., Larsen S. (1999). Calculation of broadband time histories of ground motion: Comparison of methods and validation using strong motion from the 1994 Northridge earthquake, *Bull. Seismol. Soc. Am.*, 89: 1484−1504.

Hashash Y.M.A., Kottke A.R., Stewart J.P., Campbell K.W., Kim B., Rathje E.M., Silva W.J. (2014a). Reference-rock site conditions for Central and Eastern North America: Part I − Velocity Definition, *PEER Report 2014-No. 11*, Pacific Earthquake Engineering Research Center, University of California, Berkeley, CA, 188 pgs.

Hashash Y.M.A., Kottke A.R., Stewart J.P., Campbell K.W., Kim B., Rathje E.M., Silva W.J. (2014b). Reference rock site condition for central and eastern North America, *Bull. Seismol. Soc. Am.*, 104: 684–701.

Hassani B. Atkinson G.M. (2014). Referenced empirical ground-motion model for eastern North America, *Seismol. Res. Lett.* (in review).

Herrmann R.B. (1985). An extension of random vibration theory estimates of strong ground motion to large distances, *Bull. Seismol. Soc. Am.*, 75: 1447–1453.

Hough S.E. (2014a). Earthquake intensity distributions: a new view (abstract), *Seismol. Res. Lett.,* 85: 526–527.

Hough S.E. (2014b). Shaking from injection-induced earthquakes in the central and eastern United States, *Bull. Seismol. Soc. Am.*, 104: 2619–2626.

Idriss I.M. (2014). An NGA-West2 empirical model for estimating the horizontal spectral values generated by shallow crustal earthquakes, *Earth. Spectra*, 301(3): 1155–1177.

Joyner W.B., Boore D.M. (1993). Methods for regression analysis of strong motion data, *Bull. Seismol. Soc. Am.*, 83: 469–487.

Joyner W.B., Boore D.M. (1994). Errata: Methods for regression analysis of strong-motion data, *Bull. Seismol. Soc. Am.* 84: 955-956

Kamai R., Abrahamson N.A., Silva W.J. (2013). Nonlinear horizontal site response for the nga-west2 project, *PEER Report 2013/12*, Pacific Earthquake Engineering Research Center, University of California, Berkeley, CA, 69 pgs.

Kottke A., Rathje E., Boore D.M., Thompson E., Hollenback J., Kuehn N., Goulet C.A., Abrahamson N.A., Bozorgnia Y., Der Kiureghian A., Silva W.J., Wang X. (2015). Selection of random vibration procedures for the NGA East Project, PEER report, *in preparation*.

Kottke A.R., Rathje E.M. (2008). Technical manual for Strata, *PEER Report 2008/10*, Pacific Earthquake Engineering Research Center, University of California, Berkeley, CA, 95 pgs.

Ktenidou O.J., Cotton F., Abrahamson N.A., Anderson J.G. (2014). Taxonomy of κ: A review of definitions and estimation approaches targeted to applications, *Seismol. Res. Lett.*, 85: 135–146.

Leonard M. (2010). Earthquake fault scaling self-consistent relations of rupture length, width, average displacement and moment release, *Bull. Seismol. Soc. Am.*, 100: 1971–1988.

Liu P., Archuleta R., Hartzell S.H. (2006). Prediction of broadband ground motion time histories: Frequency method with correlation random source parameters, *Bull. Seismol. Soc. Am.*, 96: 2118–2130.

Maechling P.J., Silva F., Callaghan S., Jordan T.H. (2015). SCEC broadband platform: system architecture and software implementation, *Seismol. Res. Lett.*, 86(1): 27–38.

Mai P.M., Beroza G.C. (2000). Source scaling properties from finite-fault rupture models, *Bull. Seismol. Soc. Am.*, 90(3): 604–615.

Mai P.M., Beroza G.C. (2002). A spatial random field model to characterize complexity in earthquake slip, *J. Geophy. Res.*, 107(B11): 1–21.

Mai P.M., Imperatori W., Olsen K.B. (2010). Hybrid broadband ground-motion simulations: combining long-period deterministic synthetics with high-frequency multiple S-to-S backscattering, *Bull. Seismol. Soc. Am.,* 100(5): 2124–2142.

Mai P.M., Spudich P., Boatwright J. (2005). Hypocenter locations in finite-source rupture models, *Bull. Seismol. Soc. Am.*, **95**: 965–980.

Malagnini L., Mayeda K., Uhrhammer R., Akinci A., Herrmann R.B. (2007). A regional ground-motion excitation/attenuation model for the San Francisco region, *Bull. Seismol. Soc. Am.*, 97: 843–862.

Mena B., Mai P.M., Olsen K.B., Purvance M.D., Brune J.N. (2010). Hybrid broadband ground-motion simulation using scattering Green's functions: Application to large-magnitude events, *Bull. Seismol. Soc. Am.*, 100(5A): 2143–2162.

Mitchell B.J., Hwang H J. (1987). Effect of low Q sediments and crustal Q on Lg attenuation in the United States, *Bull. Seismol. Soc. Am.*, 77: 2095–2123.

Mooney W., Chulick D.G., Ferguson A., Radakovich A., Kitaura K., Detweiler S. (2012). NGA-East: Crustal Regionalization. *NGA-East Working Meeting: Path and Source Issues*, Oct. 16 2012, University of California, Berkeley, CA.

Mooney W. (2013). *Personal Communication.*

Motazedian D., Atkinson G.M. (2005). Stochastic finite-fault modeling based on a dynamic corner frequency, *Bull. Seismol. Soc. Am.*, 95: 995–1010.

NEHRP (2000). *NEHRP Recommended provisions for seismic regulations for new buildings and other structures, Part 1, Provisions, FEMA 368*, Federal Emergency Management Agency, Washington, D.C.

Nuttli O.W., Herrmann R.B. (1984). Ground motion of Mississippi Valley earthquakes, *J. Tech. Topics* Civil *Eng.*, 110: 54–69.

Ogweno L.P., Cramer C.H. (2014). Regression relationships between modified Mercalli intensities and ground motion parameters (abstract), *Program and Abstracts, 86th annual meeting, Eastern Section of the Seismological Society of America*, Charleston, SC.

Ojo S., Mereu R. (1986). The effect of random velocity functions on the travel times and amplitudes of seismic waves, *Geophys. J. Royal Astro. Soc.,* 84: 607–618.

Olsen K.B. (2012). 3D broadband ground motion estimation for large earthquakes on the New Madrid seismic zone, Central US, *Final Report to the U.S. Geological Survey*, *Award # G10AP00007.*

Olsen K.B., Takedatsu R. (2015). The SDSU broadband ground-motion generation module BBtoolbox Version 1.5. *Seismol. Res. Lett.*, 86(1): 81–88.

Ou G.-B., Herrmann R.B. (1990). A statistical model for ground motion produced by earthquakes at local and regional distances, *Bull. Seismol. Soc. Am.,* 80: 1397–1417.

Pasyanos M.E. (2011). A case for the use of 3D attenuation models in ground-motion and seismic-hazard assessment, *Bull. Seismol. Soc. Am.*, 101: 1965–1970.

Pasyanos M.E. (2013). A lithospheric attenuation model of North America, *Bull. Seismol. Soc. Am.*, 103: 3321–3333.

Petersen M.D., Moschetti M.P., Powers P.M., Mueller C.S., Haller K M., Frankel A.D., Zeng Y., Rezaeian S., Harmsen S.C., Boyd O.S., Field N., Chen R., Rukstales K.S,, Luco N., Wheeler R.L., Williams R.A., Olsen A.H (2014). Documentation for the 2014 update of the United States national seismic hazard maps: *U.S. Geological Survey Open-File Report* 2014–1091, 243 pgs.

Pezeshk S., Zandieh A., Tavakoli B. (2011). Hybrid empirical ground-motion prediction equations for eastern North America using NGA models and updated seismological parameters, *Bull. Seismol. Soc. Am.*, 101: 1859–1870.

Power M., Chiou B.-S.J., Abrahamson N.A., Bozorgnia Y., Shantz T., Roblee C. (2008). An overview of the NGA project, *Earthq. Spectra*, 24: 3–21.

Raoof M., Herrmann R.R., Malagnini L. (1999). Attenuation and excitation of three–component ground motion in southern California, *Bull. Seismol. Soc. Am.*, 89: 888–902.

Ripperger J., Mai P.M. (2004). Fast computation of static stress changes on 2D faults from final slip distributions, *Geophys. Res. Lett.,* 31: L18610.

Scherbaum F., Bommer J.J., Bungum H., Cotton F., Abrahamson N.A. (2005). Composite ground motion models and logic trees: Methodology, sensitivities, and uncertainties, *Bull. Seismol. Soc. Am.*, 95: 1575–1593.

Scherbaum, F., Cotton F., Staektke H. (2006). The estimation of minimum-misfit stochastic model from empirical ground-motion prediction equations, *Bull. Seismol. Soc. Am.* 96: 417–445.

Scherbaum F., Schmedes J., Cotton F. (2004). On the conversion of source-to-site distance measures for extended earthquake source models, *Bull. Seismol. Soc. Am.*, 94: 1053–1069.

Schneider J.F., Silva W.J., Stark C.L. (1993). Ground motion model for the 1989 **M** 6.9 Loma Prieta earthquake including effects of source, path and site*, Earthq. Spectra,* 9(2): 251-287.

Shahjouei A., Pezeshk S. (2013). Producing broadband synthetic time histories for Central and Eastern North America, *Proceedings, Structures Congress 2013*, pp. 1767–1776.

Shahjouei A., Pezeshk S. (2014). Synthetic seismogram simulations using a hybrid broadband ground-motion simulation approach: Application to central and eastern United States, *Bull. Seismol. Soc. Am.* (accepted).

Siddiqqi J., Atkinson G.M. (2002). Ground motion amplification at rock sites across Canada, as determined from the horizontal-to-vertical component ratio, *Bull. Seismol. Soc. Am.*, 92: 877–884.

Silva W.J., Gregor N., Darragh R.B. (2002). Development of regional hard rock attenuation relations for central and eastern North America, *Report to Pacific Engineering and Analysis*, El Cerrito, CA.

Silva W.J., Gregor N., Darragh R.B. (2003). Development of regional hard rock attenuation relations for Central and Eastern North America, Mid-continent and Gulf Coast areas. *Pacific Engineering Report*, 80 pgs.

Silva et al. (1996). See page 52.

Somerville P.G. (2006). Review of magnitude-area scaling of crustal earthquakes, *Report to Working Group on California Earthquake Probabilities*, 22 pgs., URS Corp., Pasadena, CA.

Somerville P.G., Collins N., Abrahamson N.A., Graves R.W., Saikia C. (2001). Ground motion attenuation relations for the central and eastern United States, Report to U.S. Geological Survey, *NEHRP Award No. 99HQGR0098,* 36 pgs.

Somerville P.G., Graves R.W., Collins N., Song S.-G., Ni S., Cummins P. (2009). Source and ground motion models of Australian earthquakes, *Proceedings, 2009 Annual Conference of the Australian Earthquake Engineering Society*, Newcastle, Australia.

Somerville P.G., Irikura K., Graves R.W., Sawada S., Wald D., Abrahamson N.A., Iwasaki Y., Smith N., and Kowada A. (1999). Characterizing crustal earthquake slip models for the prediction of strong ground motion, *Seismol. Res. Lett.* 70: 59–80.

Somerville P.G., McLaren J., Saikia C., Helmberger D. (1990). The 25 November 1988 Saguenay, Quebec earthquake: Source parameters and the attenuation of strong ground motion, *Bull. Seismol. Soc. Am.*, 80: 1118–1143.

Somerville P.G., Smith N., Graves R.W., Abrahamson N.A. (1997). Modification of empirical strong ground motion attenuation relations to include the amplitude and duration effects of rupture directivity, *Seismol. Res. Lett.*, 68: 199–222.

Spudich P., Xu L. (2003). Software for calculating earthquake ground motions from finite-faults in vertically varying media, In *IASPEI International Handbook of Earthquake and Engineering Seismology*, W.H.K. Lee, H. Kanamori, P.C. Jennings, and C. Kisslinger (eds.), Chapter 85.14, Academic Press, New York, pp. 1633–1634.

STAN Development Team (2014). *Stan Modeling Language Users Guide and Reference Manual, Version 2.5.0.*

Stanislavsky E. Garven G. (2002). The minimum depth of fault failure in compressional environments, *Geophys. Res. Lett.*, 29(24): 8-1–8-4.

Tavakoli B., Pezeshk S. (2005). Empirical–stochastic ground–motion prediction for eastern North America, *Bull. Seismol. Soc. Am.*, 95: 2283–2296.

Tinti E., Fukuyama E., Piatanesi A., Cocco M. (2005). A kinematic source-time function compatible with earthquake dynamics, *Bull. Seismol. Soc. Am.*, 95: 1211–1223.

Toro G.R. (1996). Probabilistic ,models of site velocity profiles for generic and site-Sspecific ground motion amplification studies, Appendix C of Silva, W.J., N. Abrahamson, G. Toro and C. Costantino. (1996). "Description and validation of the stochastic ground motion model." Report Submitted to Brookhaven National Laboratory, Associated Universities, Inc. Upton, New York 11973, *Contract No. 770573.* Available on-line at http://www.pacificengineering.org/bnl/Bnl_rpt.zip.

Toro G.R. (2002). Modification of the Toro et al. (1997) attenuation equations for large magnitudes and short distances, *Risk Engineering Technical Report*, 10 pgs.

Toro G., Abrahamson N.A., Schneider J. (1997). Model of strong ground motion in eastern and central North America: best estimates and uncertainties, *Seismol. Res. Lett.*, 68: 41–57.

Toro G.R. McGuire R.K. (1987). An investigation into earthquake ground motion characteristics in eastern North America, *Bull. Seismol. Soc. Am.*, 77(2): 468–489.

Vanmarcke E.H. (1975). Distribution of first-passage time for normal stationary random processes, ASME, *J Appl. Mech.-Trans.*, 42: 215–220.

Wald D.J., Allen T.I. (2007). Topographic slope as a proxy for seismic site conditions and amplification, *Bull. Seismol. Soc. Am.,* 97: 1379–1395.

Wells D.L., Coppersmith K.J. (1994). New empirical relationships among magnitude, rupture length, rupture width, and surface displacements, *Bull. Seismol. Soc. Am.*, 84: 974–1002.

Wessel P., Smith W.H.F. (1991). Free software helps map and display data, *EOS Trans. AGU*, 72: 441–446

Working Group on California Earthquake Probabilities (2003). Earthquake probabilities in the San Francisco Bay region, 2002–2031, *U.S. Geological Survey Open-File Report 03-214*, 235 pgs.

Yenier E., Atkinson G.M. (2014). Equivalent point-source modeling of moderate- to-large magnitude earthquakes and associated ground-motion saturation effects, *Bull. Seismol. Soc. Am.,* 104: 1458–1478.

Yenier E., Atkinson G.M. (2015a). Regionally-adjustable generic ground-motion prediction equation based on equivalent point-source simulations: Application to Central and Eastern North America, *Bull. Seismol. Soc. Am.*, submitted for review.

Yenier E., Atkinson G.M. (2015b). Modeling source and attenuation attributes of the 2010–2012 Christchurch, New Zealand, earthquakes based on equivalent point-source modeling technique in preparation.

Yenier E., Atkinson G.M. (2015c). An equivalent point-source model for stochastic simulation of earthquake ground motions in California, *Bull. Seismol. Soc. Am.*, Accepted for publication.

Zandieh A., Pezeshk S. (2015). The estimation of seismological parameters for use in a stochastic point source model for western United States using an inversion technique to match the median NGA-West2 GMPEs, *Bull. Seismol. Soc. Am.*, in preparation.

Zeng Y. (1999). *Personal Communication*.

Zeng Y., Anderson J.G., Yu G. (1994). A composite source model for computing realistic synthetic strong ground motions, *Geophys. Res. Lett.*, 21: 725–728.

Zhu L., Rivera L. (2002). Computation of dynamic and static displacement from a point source in multi-layered media, *Geophys. J. Int.*, 148: 619–627.